A Dynamic Magic Angle Spinning NMR Study of the Local Mobility of Alanine in an Aqueous Environment at the Inner Surface of Mesoporous Materials

Tal Amitay-Rosen,[†] Shifi Kababya,[‡] and Shimon Vega*[,†]

Chemical Physics Department, The Weizmann Institute of Science, Rehovot, Israel 76100, Schulich Faculty of Chemisty, Technion, Haifa, Israel 32000

Received: December 2, 2008; Revised Manuscript Received: March 5, 2009

Dynamic deuterium magic angle spinning NMR has been applied to study the slow motion of small molecules close to a silica surface. In particular, alanine-d_3 molecules dissolved in an aqueous solution were loaded into the pores of the mesoporous materials SBA-15 and MCM-41. Deuterium spectra were measured as a function of the water content of these materials and the temperature. From the analysis of these spectra and the corresponding proton spectra, using a simple molecular exchange model, relatively slow desorption rates of the binding of alanine to the inner pore surface were obtained and were correlated with the low proton concentrations at the pore surfaces.

Introduction

Molecular mobility close to surfaces is of great interest in a variety of systems, such as in molecular transport during catalysis, chromatography, and slow drug release.[1−8] In this publication, we investigate the potential of solid state NMR spectroscopy to study slow reorientational motions of guest molecules close to a wet surface. To do so, we have chosen materials with a high inner-surface area that can be loaded with an aqueous solution. Materials with such high surface areas include the important mesoporous molecular sieves that were synthesized for the first time in 1992 by Mobil Research and Development Cooperation.[9] These materials are composed of a silica network with void channels and cavities possessing relatively large inner surfaces on the order of 1000 m^2/g. Two important classes of these materials are MCM-41, of the M41S family, and SBA-15.[10] These crystalline materials constitute two-dimensional hexagonal arrays of parallel cylindrical pores of uniform size that are separated from one another by thin inner walls. Whereas the pore diameter of MCM-41 are in the range of 1.5−10 nm with smooth pore surfaces, those of SBA-15 range from 8 to 30 nm, with a possible surface roughness caused by small $(SiO_2)_n$ islands.[11,12] The silica surfaces are composed of siloxanes and silanols, which exist on the surface in single, geminal, or vicinal forms.[13,14] The siloxanes are known to be hydrophobic and will not be part of hydrogen bonds with H-donor adsorbates, whereas the silanols are hydrophilic.[13] Consequently, their concentration determines the degree of surface hydrophobicity and acidity. The catalytic activity of these materials depends on the presence of various functional groups on the inner surface as well as on the presence of these hydrophobic sites. Thus, any information about these oxygen-binding sites, such as their surface concentration and binding affinity, is important.[15,16] In contrast to surfaces of other materials, such as transition metals, semiconductors, and silicon wafers, the channels of mesoporous materials create surfaces that enclose their confined space. The small diameters of the channels can influence the dynamic properties of guest molecules (diffusion rates, melting point).[17] Therefore, getting an insight into the properties of these inner surfaces as well as the state of the guest molecule is mandatory for obtaining a better understanding of their functionality.

There have been an impressive number of studies over the last 15 years that have characterized these inner surfaces as well as the effect of confinement on the structural and dynamic properties of guest molecules. Some examples of these molecules are ethanol, hexane, benzene, toluene, isobutyric acid, and many others that were characterized by means of IR, neutron scattering, DSC, TPD, and solid state NMR techniques.[18−26] These studies show that the dynamic properties of guest molecules depend on their entrapment inside the channels and on their binding strength to the inner surfaces. Similar processes occur in biological systems, where guest−host interactions are significant at enzymatic sites.[27,28] The dynamics of water molecules embedded in confined spaces has also been studied extensively,[29−33] such as diffusion in porous media and molecular filtration in geological and industrial processes or water mobility at enzymatic sites.[27,28,34]

Although solid state NMR is known for its low sensitivity and poor resolution, it is an excellent technique for studying surface adsorption/desorption dynamics of small molecules. It is sensitive to molecular motion over a wide dynamic range and is capable of determining translational and intramolecular reorientational motion.[35,36] Slow molecular dynamics studies by NMR are conducted using mainly ^2H line shape analysis[21,24,26] and 1D and 2D spectroscopy involving nuclei such as ^{29}Si, ^{13}C, and ^{15}N.[11−20,35−38] 1D- and 2D-exchange ^2H and ^{13}C experiments on static samples and samples that rotate around an axis, making an angle of 54.7° with the external magnetic field (MAS), have been conducted to follow slow dynamics and chemical exchange processes.[38−42] Fast motions can be monitored by measuring temperature-dependent spin−lattice relaxation rates,[25] whereas pulse field gradient experiments are frequently used to study translational diffusion.[22] In this study, the spectral features of dynamic MAS NMR experiments on deuterium will be analyzed to determine slow motional processes.

As mentioned earlier, many NMR experiments have been conducted to study the interaction of guest molecules, inside mesoporous materials, with host surfaces, containing a variety

* Corresponding author E-mail: shimon.vega@weizmann.ac.il.
[†] The Weizmann Institute of Science.
[‡] Technion.

10.1021/jp810572r CCC: $40.75
Published on Web 04/09/2009

of functional groups. However, combining two types of guest molecules simultaneously interacting with the host surface has not been studied extensively. A small number of unique studies have been reported in the literature in the past few years. Concentration gradients of a mixture of two solutions, 2-propanol and cyclohexane, inside the nanochannels of MCM-41 were investigated by observing high-resolution ^{13}C NMR.[43] The interaction of crystalline ibuprofen with the pore surface of MCM-41 and its rate of desorption was investigated by means of ^{1}H, ^{13}C, and ^{29}Si MAS NMR as a model for slow drug release.[44] In an additional study, we measured the adsorption and desorption kinetics of dissolved tetra-alanine, deuterated at its methyl groups, at the inner surface of MCM-41 as a function of the water concentration with the help of ^{2}H MAS NMR.[40] Different desorption rates were obtained for different water concentrations in the pores. The bound-to-free exchange motion of the guest molecules in their aqueous environment at the MCM-41 surface was not well-understood. The development of more accurate spectroscopic methodologies is necessary before a better understanding can be expected.

In the current study, the exchange process of small solute molecules at their surface binding sites is further investigated. To improve our understanding of this process, ^{1}H and ^{2}H MAS NMR spectra were collected and correlated using a simple exchange model. In particular, deuterated alanine dissolved in water has been loaded into SBA-15 and MCM-41, and their exchange dynamics at the surface binding site were monitored. As we will show, our experiments demonstrate that single water molecules are sufficient to remove the bound alanine molecules from the surface.

In the next section, a description of the alanine exchange process is presented that will assist us to interpret our data and will ease our further discussions. This is followed by a description of the ^{2}H MAS NMR methodology that enabled the study of surface exchange processes. For the analysis of these spectra, a simple exchange model is chosen, and its validity is estimated. Then the synthesis of the SBA-15 and MCM-41 materials and the preparation of the samples loaded with an aqueous solution of alanine are described. In the last section, the results of these experiments on a set of alanine loaded samples as a function of the water content and temperature are shown. Finally, the analysis of the ^{1}H and ^{2}H MAS NMR spectra of these samples provides us with the values of the alanine exchange rates and their dependence on the number of water molecules per square nanometer bound to the pore surface and the temperature.

A General Description of the System. ***The Surface.*** Before introducing the theoretical model that will assist us to interpret our experimental results, we present here a molecular scheme for the inner surface of the mesoporous materials. This scheme is based on prior knowledge about the water formations at the surface of the pore walls in SBA-15[30] and on the inhomogeneous NMR line shapes of the protons close to the surface. To visualize our system, we consider the inner walls of the mesopores in SBA-15 or MCM-41 as SiO_2 surfaces. TEM images of our SBA-15 samples (see the Supporting Information) show that the disruption of the surface at the pore edges and the outer surface of the crystallites constitutes a minor fraction of the total surface. When these surfaces are dry, they can be interrupted by different types of local molecular distortions: single, geminal, or vicinal $-$OH groups terminating the dangling bonds of the silicon atoms as well as ordered water molecules that are bound together by hydrogen bonding networks near silanol sites on the surface.[13] We will refer to these proton$-$oxygen structures as clusters, situated around at least one oxygen site on the surface. At very low water loading, the ^{1}H spectra can be decomposed into a set of homogeneous lines, indicating that in SBA-15, we are dealing with a distribution of isolated clusters.[30] Their size distributions and compositions cannot be determined exactly. Moreover, at low water concentrations, there is no fast proton exchange between the clusters, and all reorientational motion of the water is internal. When these clusters grow, this exchange process becomes significant, and the components of the proton spectrum merge into a single spectral line. Following the cluster analysis in SBA-15 of Grunberg et al.,[30] at low water loading, these clusters contain a very small number (<6) of protons. We assume that, on average, these clusters are distributed randomly at oxygen sites on the surface. Increasing the water content will first result in a translational motion of single water molecules and eventually will result in a full coverage of most parts of the inner surface. Depending on the mesoporous material, increasing the water content in the pores will either cause the whole surface to be covered, as in SBA-15, or will first fill the pores locally, as in MCM-41.[30]

In the present study, we are interested in the relatively slow dynamics of small guest molecules induced by water molecules. At high water content, these guest molecules are dissolved in the aqueous solution that fills the pores and perform an isotropic reorientational motion. As the amount of water decreases, the majority of the molecules undergo an exchange process between surface-bound and free rotating states in solution. At very low water concentrations, this process is expected to be correlated with a process involving a very small number of water molecules that exchange with single guest molecules. In this study, we addressed questions about the number of water molecules that are needed to initiate this slow exchange process and about the minimal cluster size distribution that provides these exchanging water molecules. To answer those, we deuterated dissolved alanine molecules at their methyl sites and followed their bound-to-free exchange dynamics in the pores by measuring ^{2}H MAS NMR spectra. These spectra exhibit center and sidebands that have intensities and line widths that are sensitive to motion. The changes in these ^{2}H MAS sideband parameters will appear when the characteristic time scale of the exchange motion becomes smaller than 10^{6} s^{-1}. Thus, with this spectroscopic approach, we are restricted to relatively slow motional effects. By lowering the amount of water in our sample, we can expect to reach this slow motional regime, where the ^{2}H MAS sideband spectra of the guest molecules become sensitive to their exchange motion and exchange rates, and bound fractions can be derived. At higher rates, double quantum filtering experiments can be applied to determine free-to-bound exchange parameters.[45] In the fast motional regimes, spin relaxation measurements can assist in retrieving dynamic information.[46]

The Exchange Process. In an effort to quantify our experimental data analysis, we will correlate the alanine dynamics with the cluster size distribution. At each wetting level of the samples, we can determine the average number (p) of protons per square nanometer of pore surface. For each p value, there exists a distribution $d(p; x)$ of clusters, starting from single $-$OH groups with $x = 1$ and growing to $-OH_2^+$ with $x = 2$ and $-$OH $+$ H_2O with $x = 3$ etc. These clusters are shown schematically in Figure 1. As long as the number of guest molecules per square nanometer is significantly smaller than p, we can expect that they do not influence the overall distribution, $d(p; x)$. The presence of free water molecules that exchange with guest molecules must be associated with the cluster distribution on the surface. The deuterated guest molecules in our study result

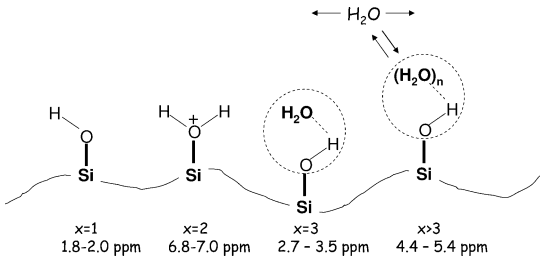

Figure 1. A schematic representation of the isolated proton clusters ($x = 1, 2,...$) at the oxygen sites on the inner SiO_2 surface of the dry mesoporous materials, together with their range of proton chemical shift values.

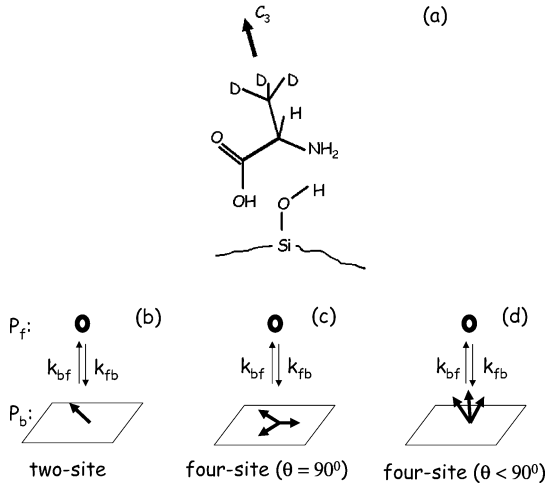

Figure 2. A schematic representation of the exchange models for the alanine molecules bound to the surface. (a) Alanine-d_3 molecule with some fixed orientation with respect to the SiO_2 inner surface is drawn with a methyl group pointing in space with a stationary CD_3 symmetry axis. The direction of this axis is represented by a bold arrow. (b) A representation of a two-site exchange model with a molecule jumping between some fixed position on the inner surface, with some arbitrary direction of its CD_3 axis; and a state of reorientaion, with zero average quadrupole coupling constant. The bound alanine molecule is replaced by a bold arrow representing its fixed CD_3-axis direction; and the free reorienting alanine, by a bold circle. The relative populations of the two states are P_b and P_f, respectively. The exchange rates k_{bf} and k_{fb} are also indicated. (c) Representation of a four-site jump model. Here, the three bound sites of the alanine molecule have their CD_3 axes in the plane of the surface ($\theta = 90$ °), making an angle of 120 ^{0} with each other. Any direct exchange between the surface sites is ignored. (d) The same as part c with $\theta < 90°$.

in ^{2}H spectra that are analyzed in terms of a dynamic process consistent with an exchange between bound and free molecules, with relative average amounts of $P_b(p)$ and $P_f(p)$, respectively. For guest molecules in the vicinity of clusters with small x values, we expect that there are not enough free water molecules that can cause an exchange motion. Thus, a fraction, $S_b(p)$, of the guest molecules will stay immobile while the remaining molecules undergo an exchange process. The process can then be defined by average desorption and adsorption rates $k_{bf}(p)$ and $k_{fb}(p)$, respectively. The number x_g of free water molecules exchanging with each guest molecule may vary, and it is not obvious that for each p value, the distribution $d(p; x_g)$ is correlated to the cluster distribution $d(p; x)$. The above-mentioned rates and fraction of immobile molecules are therefore weighted averages of the individual $k_{bf}(x_g)$ and $P_b(x_g)$ values. Thus, from our experiments, we can expect to derive only these weighted average values. Because the sample preparation and manipulations can influence the distributions $d(x)$ and $d(x_g)$, we can expect some deviations in the parameters for different samples with the same p value.

The parameters that determine the bound-to-free exchange motion of the mobile deuterated molecules are the desorption and adsorption rates $k_{bf}(p)$ and $k_{fb}(p)$ and the relative amounts of fixed and free molecules P_b and P_f, respectively. To maintain the ratio between the steady state populations of the sites, we require that

$$\frac{k_{fb}}{k_{bf}} = \frac{P_b}{P_f} \tag{1}$$

with $P_f + P_b = 1$. To define the dynamic parameters of the exchange process, we have chosen the two independent parameters k_{bf} and P_b. A similar model for bound-to-free molecular exchange has also been introduced for the study of water at the surface of proteins.[47,48]

Dynamic ^{2}H MAS NMR. ***The Surface Exchange Model.*** In this section, we focus on the description and analysis of ^{2}H MAS sideband patterns that were obtained from our NMR experiments on deuterated alanine molecules inside SBA-15 and MCM-41. As in static samples, these spectra provide information on slow reorientational dynamics, such as rotational diffusion and chemical exchange.[21,49−51] Although the dynamic MAS spectra are less sensitive to these motions than their nonspinning counterparts, they enable us to study the slow motions of samples containing very low abundance deuterons with very small signal-to-noise ratios in static experiments. Off magic angle spinning measurements were also performed, and their powder spectra were analyzed in terms of slow motional processes using Floquet theory.[52,53] The ^{2}H sideband spectra are determined by the nuclear quadrupole interaction, described in the rotating frame MAS Hamiltonian as

$$H(t) = \omega_Q(t)\left(I_z^2 - \frac{1}{3}I(I+1)\right) \tag{2}$$

where the time dependence results from the sample rotation. The instantaneous frequency values $\omega_Q(t)$ of the $|1\rangle \rightarrow |0\rangle$ and $|0\rangle \rightarrow |-1\rangle$ transitions of a deuterium nucleus with spin-1 in a rotating single crystal with a quadrupole tensor defined by a quadrupole coupling constant $\omega_Q = e^2qQ/\hbar$ and an asymmetry parameter η are given by[54]

$$\omega_Q^{\pm}(t) = \pm\omega_Q \sum_{n=-2}^{2} g_n(\alpha, \beta, \gamma; \eta) e^{in\omega_r t} \tag{3}$$

where α, β, γ are the initial Euler angles of the principal axis system of the quadrupole tensor with respect to the spinning-rotor frame; g_n is the geometric coefficients that are functions of those angles; and η and ω_r are the asymmetry parameter and the sample spinning frequency. In organic compounds, the values of $\nu_Q = \omega_Q/2\pi$ for immobile deuterium nuclei range from 140 to 240 kHz.[55] The shapes of the centerband and sidebands in ^{2}H MAS spectra are sensitive to molecular motions with characteristic rates that are smaller or comparable to the strength of these quadrupole interactions. Thus, the characteristic time constants of these motions must be longer than 10^{-6} s, as mentioned earlier.[35] Sideband patterns have been analyzed to determine rate constants of rotational diffusion and molecular jump motions.[40,42,53]

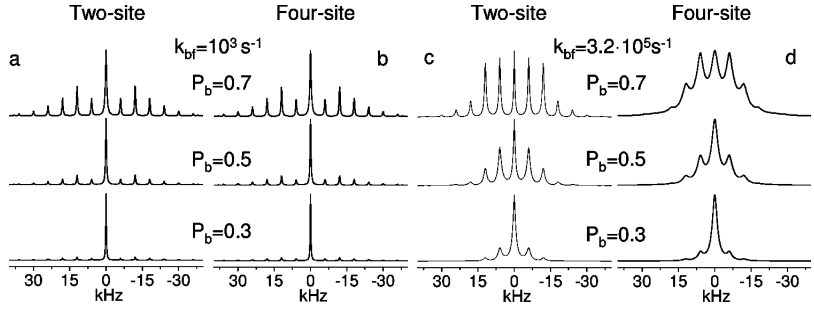

Figure 3. Simulated ^{2}H MAS spectra for $k_{bf} = 10^3$ and 3.2×10^5 s^{-1}, and varying P_b values, using the two-site (a, c) and four-site (b, d) exchange model with $\theta = 90°$. During these calculations, the values of ν_Q and ν_r were 51 and 6 kHz, respectively.

In our study, the changes in the ^{2}H MAS NMR line shapes of dissolved CD_3-labeled alanine molecules originate from the restrictions of their reorientational motion imposed by the pore walls. As we will show, the changes in our spectra can be analyzed by assuming a two-state exchange process of the solute molecules jumping between a free isotropically reorientational state and a stationary state. At the static state, the molecules are attached to the surface walls, allowing only the fast methyl motion around their CD_3 symmetry axes. This exchange process is a function of the number of nearby water molecules and the temperature. In the absence of motion, when all molecules are unable to move at the surface, a well-defined narrow static sideband pattern, determined by the effective CD_3 quadrupole coupling constant ω_Q and $\eta = 0$ is obtained. The principal axis of the corresponding effective quadrupole tensor can point in different directions with respect to the surface wall, depending on the binding characteristics of the alanine molecules to the surface. Because the OH groups of the silanols binding sites at the surface rotate freely around their Si-O bonds, we expect that the possible orientations of the principal axes of the CD_3 groups of alanine at these sites are correlated by cylindrical symmetry around the local norm to the surface. Thus, all principal axes of the bound molecules make an angle θ with this norm. In the fast exchange limit, an average narrow-line spectrum is obtained that corresponds to a tensor with a quadrupole coupling constant $P_b(3\cos^2\theta - 1)\omega_Q$. In the very slow motional regime, the spectrum will look like a superposition of two spectra: one of a broadened static MAS spectrum corresponding to ω_Q and one broadened centerband originating from the free reorienting molecules.

To analyze the changes in the dynamic spectra, we must assume a dynamic model that represents the surface exchange process and that can be characterized numerically. In the slow motional regime, a relatively small number of water molecules can induce an exchange process of the guest molecules at their binding site. When water molecules exchange with these guest molecules, they cause these molecules to reorient freely at least part of the time. During that time, we assume that the characteristic rate of reorientation is much faster than the quadrupole interaction strength of the static molecules. Thus, this two-state exchange process exists of molecules jumping between one state with relative population $(1 - P_b)$ and an effective quadruple coupling constant $\nu_Q = 0$ and another bound state with relative population P_b and a nonzero ν_Q. The quadrupole tensor axis of the bound state points in some direction, making some fixed polar angle θ with the norm to the surface and an arbitrary azimuthal angle.

To check when it is allowed to replace this two-state exchange process by a two-site exchange model, where we consider only one arbitrary binding site, we must show that the experimental spectra are independent of the tensor orientations of the molecules at these binding sites. To do so, we compared the two-site exchange model (i.e., the exchange of methyl deuterons between one site with a fixed static tensor and one site with a zero tensor) with four-site exchange models. These models consist of one isotropically reorientational site and three static sites with equal quadrupole coupling constants. In Figure 2, these exchange models are drawn schematically. The main principal axes of these three bound sites are correlated by a C_3 rotation perpendicular to the surface, all making a fixed angle θ with the norm to the surface. These sites present a simplified model for tensors of molecules bound to a surface, assuming that their orientations are correlated by cylindrical symmetry. Molecules in the reorientational site can, of course, experience some translational motion, as well. As will be shown, the line shapes of these simple models can be calculated rather easily, and different values for θ can be considered. When the main axes of the three axial tensors are perpendicular to the surface ($\theta = 0$), the four-site model becomes identical to the two-site case. An optimal fitting procedure between experimental and simulated sideband spectra can provide the relative populations P_b and the exchange rates of desorption k_{bf} for these exchange models.

Floquet Theory for the Four-Site Model. ^{2}H MAS spectra are simulated using the Floquet theory approach describing the multisite exchange motion in rotating samples.[39,53,56,57] Free induction decay signals of the exchanging deuterons are obtained by solving the McConnel equation in Floquet space and are being Fourier transformed to yield sideband patterns that can be compared with experimental data. Assuming that there are no interactions between spins at the different sites, the infinite dimensional rate equations for the single quantum transverse magnetization Floquet vectors at each site have the form

$$\frac{d}{dt}\begin{pmatrix}\bar{m}_{\pm}^{I}(t)\\ \bar{m}_{\pm}^{II}(t)\\ \bar{m}_{\pm}^{III}(t)\\ \bar{m}_{\pm}^{IV}(t)\end{pmatrix} = \Gamma_F\begin{pmatrix}\bar{m}_{\pm}^{I}(t)\\ \bar{m}_{\pm}^{II}(t)\\ \bar{m}_{\pm}^{III}(t)\\ \bar{m}_{\pm}^{IV}(t)\end{pmatrix} \qquad (4)$$

where the infinite dimensional vectors $\{m_{+,n}^{I-IV}(t)\}_{n=-\infty}^{\infty}$ correspond to the $|1\rangle \leftrightarrow |0\rangle$ transitions of the $I = 1$ spins at sites I−IV; and $\{m_{-,n}^{I-IV}(t)\}_{n=\infty}^{\infty}$, to the $|0\rangle \leftrightarrow |-1\rangle$ transitions at these sites. The infinite Floquet relaxation matrix equals

$$\Gamma_F^{\pm} = \begin{pmatrix} -iH_F^{I\pm} - k_{fb}\mathbf{1} & (k_{bf}/3)\mathbf{1} & (k_{bf}/3)\mathbf{1} & (k_{bf}/3)\mathbf{1} \\ (k_{fb}/3)\mathbf{1} & -iH_F^{II\pm} - (k_{bf}/3)\mathbf{1} & 0 & 0 \\ (k_{fb}/3)\mathbf{1} & 0 & -iH_F^{III\pm} - (k_{bf}/3)\mathbf{1} & 0 \\ (k_{fb}/3)\mathbf{1} & 0 & 0 & -iH_F^{IV\pm} - (k_{bf}/3)\mathbf{1} \end{pmatrix} \quad (5)$$

where $\mathbf{1}$ is an infinite unit matrix and k_{fb} and k_{bf} are the adsorption and desorption rate constants. In the on-resonance rotating frame, for each set of Euler angles, the elements of the single-site Floquet spin Hamiltonians are equal to

$$H_F^{II-IV\pm} = \pm\omega_Q \sum_{n=-2,n\neq 0}^{2} g_n^{II-IV}(\alpha,\beta,\gamma;\eta)\, F_n^{II-IV} + \omega_r N^{II-IV} \quad (6)$$

$$H_F^{I} = \omega_r N^{I} \quad (7)$$

where site I corresponds to the free reorientational site with an effective quadrupole interaction equal to zero and II−IV corresponds to the three static sites. Here, the sample spinning frequency is equal to ω_r, and F_n and N are the ladder and the number Floquet operators, respectively.[58] Furthermore, we assume that all deuterons have the same chemical shift value. The trigonometric coefficients are correlated via a simple 3-fold rotation:

$$g_n^{II}(\alpha,\beta,\gamma) = \sum_{n'} D_{nn'}^{(2)}(\alpha,\beta,\gamma)\, d_{0n'}^{(2)}(\theta) \quad (8)$$

$$g_n^{III}(\alpha,\beta,\gamma) = \sum_{n'} D_{nn'}^{(2)}(\alpha,\beta,\gamma)\, d_{0n'}^{(2)}(\theta)\, e^{i2n'\pi/3} \quad (9)$$

$$g_n^{IV}(\alpha,\beta,\gamma) = \sum_{n'} D_{nn'}^{(2)}(\alpha,\beta,\gamma)\, d_{0n'}^{(2)}(\theta)\, e^{-i2n'\pi/3} \quad (10)$$

where θ is again the angle between the norm to the surface and the directions of the symmetry axis of the quadrupole tensors with $\eta = 0$. Here, $D_{nn'}^{(2)}(\alpha,\beta,\gamma)$ are second-order Wigner matrix elements, and $d_{nn'}^{(2)}(\theta)$ are their reduced elements. The solution of eq 4 requires diagonalization of the infinite matrices $\Gamma_F^{\pm}$. Because these two matrices differ only in the sign of the off-diagonal elements in $H_F^{II-IV\pm}$, the diagonalized matrices are identical, and the diagonalization matrices satisfy $D_F^{\pm} = (D_F^{\mp})^{-1}$:

$$\Gamma_F^{\pm} = (D_F^{\pm}) \begin{pmatrix} i\omega_r N^{I} - k^{I}\mathbf{1} & & & \\ & i\omega_r N^{II} - k^{II}\mathbf{1} & & \\ & & i\omega_r N^{III} - k^{III}\mathbf{1} & \\ & & & i\omega_r N^{IV} - k^{IV}\mathbf{1} \end{pmatrix} (D_F^{\pm})^{-1} \quad (11)$$

In practice, the diagonalization is performed on a truncated matrix of dimension $4N_{max} \times 4N_{max}$, where N_{max} is chosen according to the magnitude of ω_Q/ω_r. The diagonalization for each (α, β, γ) results in four rate constants, k^{I-IV}.

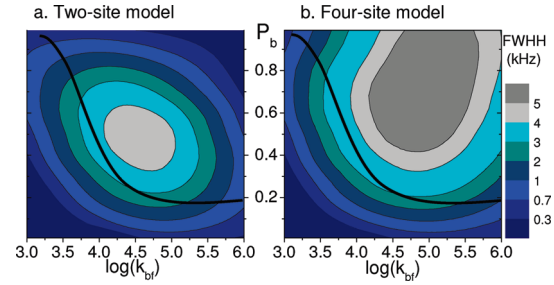

Figure 4. Contours of the fwhh of the centerband of ^{2}H MAS spectra as a function of log(k_{bf}) and P_b for $\nu_Q = 51$ and $\nu_r = 6$ kHz using the two-site (a) and the four-site exchange model with $\theta = 90°$ (b). Below the solid line, the two contours are about equal.

The time-dependent signal of the exchanging deuterons is given by

$$S(t) = \int\int\int da \sin\beta\, d\beta\, d\gamma \sum_{\Sigma=I,II,III,IV} \sum_{n=-\infty}^{\infty} \{m_{+,n}^{\Sigma}(t) + m_{-,n}^{\Sigma}(t)\} e^{inw_r t} \quad (12)$$

and the magnetization vectors are calculated according to

$$m_{\pm n}^{\Sigma}(t) = \sum_{\Xi=I,II,III,IV} \sum_{n'} \langle n,\Sigma|D_F^{\pm}|n',\Xi\rangle \times \langle n',\Xi|D_F^{\pm -1}|0,\Sigma\rangle e^{in'\omega_r t} e^{-k^{\Xi}t} \quad (13)$$

These calculations yield powder signals $S(t)$ for each set of exchange rates and initial values of $m_{+,0}^{I-IV}(0)$. After Fourier transformation of these signals, symmetric sideband MAS spectra are obtained with relative intensities that are determined by the elements of D_F and the rates k^{I-IV}. A more elaborate discussion of the solution of the rate equations in Floquet space can be found in references 49 and 50.

A Comparison between the Two- and Four-Site Exchange Models. To conduct a comparative study of the two- and four-site exchange models, we simulated a set of spectra for varying k_{bf} and P_b values. In Figure 3, some of these simulated spectra are shown for two k_{bf} values. It is clearly seen that for $k_{bf} = 10^3$ s^{-1}, the two models result in similar spectra as a function of P_b, whereas for $k_{bf} = 3.2 \times 10^5$ s^{-1}, the two sets of spectra differ significantly. To conduct a comparison between the spectra of the two models, two parameters were chosen: the line width of the centerband and the ratio between the intensities of the first sideband (I_1) and centerband (I_0). Contour plots of the full width at half-height (fwhh) of the centerband of the MAS spectra as a function of the {log (k_{bf}), P_b} parameters are shown in Figure 4. The intensity ratios I_1/I_0 are not added here to prevent crowding of the contours. Contours presenting these ratios, accompanied by an additional plot of some ratios at different P_b values, are added to the Supporting Information. The contours and intensity ratios were calculated using an effective quadrupole coupling constant of 51 kHz, which is a typical value for a CD_3 group, and a spinning frequency of 6 kHz. In the four-site case, the CD_3 symmetry axes of the three methyl groups at their static sites are pointing in the plain of the surface ($\theta = 90°$). A simple inspection reveals that in the region below the solid lines in Figure 4, the spectra for the two- and four-site exchange models are about the same, allowing a variance of 20% in the line width and in the I_1/I_0 ratio. As long as the parameters of our spin system are in this range, we can analyze the data using the two-

site model. The degree of precision of the two-site exchange model was evaluated and is demonstrated in a contour plot in the Supporting Information. Accordingly, the accuracy in k_{bf} and P_b depend on their values, and is as follows: For log (k_{bf}) < 4.5, it is ± 0.15, and for log (k_{bf}) > 4.5, it is ± 0.4; it is ± 0.03 for $P_b > 0.2$ and ± 0.01 for $P_b < 0.2$. Inspection of contour plots for different θ values shows that for the values {k_{bf}, P_b} below the solid lines in Figure 4, the line widths and intensity ratios are about independent of θ. A contour plot for $\theta = \pi/4$ has been added to the Supporting Information. A closer look at the calculated spectra reveals, however, very small variations in the intensities of the higher-order sidebands, especially at high exchange rates, as a function of θ. The similarity of the spectra below the solid line is, indeed, quite obvious. Since sites II, III, and IV are not connected directly by jumps, at small values of k_{bf}, the molecules reside at their bound state long enough for their coherences to accumulate phases that result in defined frequency components in the spectra. Thus, the averaging process of these frequencies, of molecules residing at consecutive bound sites, is not sufficient, even for small P_b values. This changes when the residence time at the sites shortens and the frequency averaging becomes significant. For small P_b values and increasing k_{bf}, the molecules reside in the isotropic site most of the time, and the spectra are mainly characterized by a broadened centerband.

To demonstrate the sensitivity of the dynamic MAS spectra to changes in the quadrupole coupling constant and spinning rates, we calculated an additional contour for $\nu_Q = 160$ kHz and $\nu_r = 10$ kHz and added it to the Supporting Information. This quadrupole coupling constant corresponds to the $C_\alpha D$ group in an amino acid. In this contour and in those of Figure 4, all line widths larger than half the spinning frequency are not shown explicitly. Using the two-site model, accurate data analysis will be possible only in the fast and slow motional regimes or for small and large P_b values. When $\nu_Q = 51$ kHz, the values of k_{bf}, for which the dynamic MAS spectra are sensitive to changes in the exchange rates, are smaller than 3.1×10^3 or larger than 1.6×10^5 for all P_b values and $3.1 \times 10^3 \leq k_{bf} \leq 10^6$ s^{-1} for $P_b \leq 0.2$ or ≥ 0.7. These values change and becomes smaller when ν_Q increases to 160 kHz: $k_{bf} < 3.1 \times 10^3$ for all P_b values and $3.1 \times 10^3 < k_{bf} < 10^6$ s^{-1} for $P_b \leq 0.1$ or ≥ 0.8. These restrictions on the spectral sensitivity to changes in {k_{bf}, P_b} limits our ability to study larger variations in k_{bf}.

In practice, the experimental spectra must be fit to simulated spectra to obtain k_{bf} and P_b values. Assuming that we know the value of ν_Q, these parameters can first be estimated by comparing the experimental line widths and the experimental I_1/I_0 ratios with those in the contour plots. As long as these values fall within the range of parameters below the solid line in Figure 4, an actual best-fitting procedure must be performed. If the parameters are outside the overlapping region, we must repeat the whole procedure using one of the four-site exchange models or more complicated ones. This procedure is not straightforward due to the angle-θ dependence. Fortunately, such simulations were not necessary in our present study, and all MAS spectra could be analyzed reasonably reliably, despite their low signal-to-noise ratios.

A spectral feature of all MAS sideband spectra of these two- and four-site exchange models is the appearance of an intense centerband. This feature is characteristic for an exchange process with one isotropic site. Other exchange models will not exhibit a dominant centerband at a wide range of rate constants. For example, when all four sites have nonzero effective quadrupole tensors, although their frequencies and orientations average to zero in the fast exchange limit, their dynamic spectra do not show the strong centerband appearance. A set of simulated spectra for such a case is also added to the Supporting Information.

In the following discussion, we will restrict ourselves to the two-site exchange model for the analysis of our experimental ^{2}H MAS NMR data and show that the resulting exchange parameters {k_{bf}, P_b} fall below the solid line in Figure 4.

Materials and Methods

Data Analysis and Simulations. Two-site exchange MAS ^{2}H line shapes were calculated for $\nu_Q = 51$ and 160 kHz with k_{bf} values in the range of $310-10^6$ s^{-1} and spinning frequencies equal to 6 or 10 kHz, respectively. The truncated dimension of the Floquet matrix depends on the size of the quadrupole interaction and was set to $N_{max} = 31$ and 51, respectively. In both cases, the powder averaging was performed by the ZCW algorithm for 1154 crystal orientations. For the four-site exchange models, ^{2}H MAS line shapes were calculated using $\nu_Q = 51$ kHz for the same k_{bf} values as mentioned above and with a spinning frequency of 6 kHz. The dimension of the Floquet matrix block was set to $N_{max} = 25$, and the calculation was repeated for 512 crystal orientations, with the same tiling scheme mentioned above. In all cases, the FID signals consisted of 512 data points and were Fourier transformed to yield frequency domain spectra. All simulations were performed using a Fortran program written by R. Poupko and were run on an Alpha Server ES40. The necessary CPU time for a single spectrum calculation depends on the size of the quadrupole coupling constant, the size of the Floquet matrix block, the number of crystal orientations, and the number of FID points. In the case of two-site exchange, with $\nu_Q = 51$ kHz, 1154 crystal orientations, and 512 FID points, the CPU time is about 15 min, whereas for the four-site exchange model, it is about 5 times longer.

Where necessary, the experimental ^{2}H MAS NMR spectra of the guest molecules were deconvoluted into distinct spectral components using the DMFIT program.[59] Almost all our sideband spectra consisted of a broad and a narrow constituent. The broad parts were analyzed as described above, and the best-fit spectra provided the k_{bf} and P_b values. The narrow sideband patterns, which characterize deuterons with a static quadrupole coupling constant equal to 51 kHz, correspond to guest molecules that are bound to the surface wall and do not participate in any exchange process. The relative amounts of these molecules are denoted by the parameter S_b. It is determined by the ratio between the intensities of these static sideband spectra and the total spectra after deconvolution. The overall spectral width and sideband intensities of the static spectra determine the quadrupole coupling constant of the guest in their bound state.

Materials

Preparation of Mesoporous Materials. ***Preparation of SBA-15.*** SBA-15 was prepared in an acidic environment according to a procedure reported earlier.[60] A 14 g portion of poly(ethylene glycol)−block-poly(propylene glycol)−block-poly(ethylene glycol) triblock copolymer (Aldrich, $H(-OCH_2CH_2)_x[-OCH(CH_3)-CH-]_y(-OCH_2CH_2-)_zOH$), $M_{avg} = 5800$) was dissolved by stirring in 447 mL of water and 66 mL of 32 wt % HCl for 1 h at 50 °C, followed by addition of 21.7 g of tetramethylorthosilicate and stirring for 10 min. The solution was then transferred into a Teflon reactor and stirred first at 60 °C for 24 h and then at 100 °C for another 24 h. After cooling to room

TABLE 1: Surface Properties of SBA-15 and MCM-41 Obtained from N_2 Adsorption Measurements

material	surface area (m^2 g^{-1})	pore volume (cm^3 g^{-1})	mean pore diameter (Å)
SBA-15	849.2 (BET)	11.3 (BJH)	159.1 (BJH)
MCM-41	1458 (BET)	1.4 (BJH)	38 (BJH)

temperature, the solid product was recovered by filtration. Calcination in air at 300 °C for 2 h, 400 °C for 2 h, and 500 °C for 6 h (with a slow temperature increase of 1 °C/min) completed the preparation.

Preparation of MCM-41. MCM-41 was prepared according to a procedure reported earlier.[61] A liquid mixture composed of SiO_2/0.21 cetyltrimethylammoniumchloride (CTAC)/0.21 Na_2O/0.02 $(NH_2)_4O$/89 H_2O was stirred vigorously in a plastic beaker for 1 h at room temperature. The resulting gel was transferred to a Teflon-coated autoclave and maintained at 97 °C for 24 h. Then the autoclave was cooled in an ice bath, and the pH was adjusted to 10.2 by adding 30% acetic acid. NaCl (8.34 g, Aldrich) was then added to the gel, followed by stirring at room temperature for 1 h. The heating at 97 °C, cooling, and pH adjustment (without NaCl addition) procedures were repeated three times. The resulting product was obtained by suction filtration, then it was dried at 120 °C for 2 h and calcined in air at 300 °C for 2 h and at 530 °C for another 6 h.

Characterization of SBA-15 and MCM-41. N_2 adsorption/desorption isotherm measurements were conducted on samples of calcined SBA-15 and MCM-41 with a NOVA-2000 (Quantachrome, version 7.01) apparatus. The surface area, pore volume, and pore diameter were obtained from the isotherms using the BET and BJH methods and are summarized in Table 1. It is important to note that SBA-15 also contains micropores, which are positioned inside the walls between the mesopores. However, in our case, these micropores are only 3% of the surface area of the material and can be neglected.

Sample Preparation. ***SBA-15 Loaded with 1:1 H_2O/D_2O Solution.*** Sixty milligrams of calcined SBA-15, which was initially heated to 200 °C for two hours (to remove residual water), was added to a mixture of 1.5 mL of H_2O and 1.5 mL of D_2O. A similar sample was prepared with the addition of 50 mg nondeuterated alanine (alanine-h_3) to the 1:1 3 mL of D_2O/H_2O mixture. The suspensions were stirred for 30 min, and 3 h, respectively, at room temperature and then filtered. Before being packed inside the NMR rotor, the material was allowed to dry in air for approximately 3 h to remove water situated at the external surface of the samples.

SBA-15 Loaded with an Aqueous Solution of Alanine-d_3. Sixty milligrams of calcined SBA-15, which was initially heated to 200 °C for 2 h (to remove residual water), was added to a solution of 61 mg of DL-alanine-d_3 purchased from Cambridge Isotope Laboratories, Inc., and dissolved in 1.5 mL of H_2O (0.44 M). The suspension was stirred for 3 h at room temperature. The mixture was then filtered, and the remaining powder was allowed to dry in air for approximately 3 h to remove water situated on the external surfaces of the drying sample. The remaining powder was then packed inside the NMR rotor. We assume that the concentration of the guest molecules inside the pores during the sample preparation is similar to that in the initial solution. Residual alanine molecules that are located outside the pores form a very small fraction of the alanine in the sample.

To ensure that the solution was inserted inside the pores of SBA-15 during the mixing period, an additional sample was prepared by an alternative procedure, by which 60 mg of SBA-15 was dried for 2 h under vacuum at 130 °C prior to the addition of the guest solution, which was added to the sample under vacuum. A comparison between spectra of samples that were prepared in both ways showed very similar ^1H and ^2H MAS spectra.

MCM-41 Loaded with an Aqueous Solution of Alanine-d_3. Fifty milligrams of calcined MCM-41, which was initially heated to 200 °C for 2 h, was added to a solution of 59 mg of DL-alanine-d_3, purchased from Cambridge Isotope Laboratories, Inc., in 1.5 mL of H_2O (0.42 M). The suspension was stirred for 3 h at room temperature. The mixture was then filtered and allowed to dry in air for approximately 3 h to remove water situated on external surfaces. Then the sample was packed inside the NMR rotor. When the pores are saturated with the solution, we expect that the concentration of the guest molecules inside the pores is similar to that of the initial solution.

In all stages during the experiment, the amount of water inside the pores was controlled by exposing the sample inside the rotor to a low pressure of 10^{-6} Torr after removing its sample cap and by pumping for certain time periods. The residual amount of water was determined by the linear dependence of the remaining integrated intensity of its ^1H spectra on the weight of the sample. Reduction and addition of solvent under vacuum was found to be reproducible in terms of the relation between the weight loss/gain and the intensity decrease/increase. The linear dependence between the integrated ^1H intensity and the weight loss/gain of the sample will be shown in the following section.

NMR Measurements. ^1H, ^2H, and ^{29}Si NMR measurements were performed on a Bruker DSX spectrometer operating at 300.13, 46.07, and 59.6 MHz, respectively. This spectrometer was equipped with a Bruker 4 mm MAS probe. The sample temperature was controlled by a Bruker variable temperature controller, with a temperature stability of ±1 K and calibrated using ^{207}Pb.[62] For each temperature, the tuning and matching of the coil were optimized. ^1H MAS NMR experiments were carried out at spinning frequencies equal to 6 or 10 kHz. A spin−echo pulse sequence, with a 90° excitation pulse of 3.95 μs and an echo delay of either 160 or 94.8 μs, respectively, was used to collect the proton spectra. The repetition delay of these experiments was 4 s. The pulse length and the chemical shift parts per million scale (ppm) were calibrated using an adamantane sample.

^2H MAS NMR measurements were conducted by applying a 90° excitation pulse of 2.8 μs, which was calibrated using a standard sample of uniformly deuterated hexamethyl benzene. The spinning frequency of these experiments was 6 kHz, and their repetition delay was 0.3 s. Up to about 30 000 accumulations were necessary to obtain a reasonable signal-to-noise ratio. Due to the exchange motion, the time domain signals decay with some characteristic time that broadens the center and sidebands. From the start of this free induction decay signal until the start of the signal accumulation, at the first rotor echo position, some intensity is lost, causing a loss of intensity of the Fourier transformed frequency spectrum, as well. In our data analysis, this signal loss has been taken into account, and all integrated spectral intensities are corrected accordingly. This is done by searching for the best $\{k_{bf}, P_b\}$ parameters, comparing experimental and simulated spectra, and calculating the intensity loss using these optimal parameters.

^{29}Si MAS NMR experiments were carried out at a spinning frequency of 5 kHz, employing a spin−echo pulse sequence with a 90° excitation pulse of 4.4 μs, an echo delay of 200 μs,

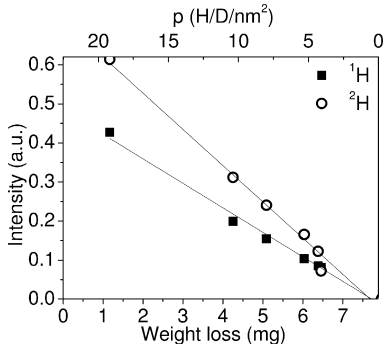

Figure 5. Total integrated intensities (in arbitrary units) of the ^{1}H (squares) and ^{2}H (circles) spectra of a 1:1 mixture H_2O/D_2O inside SBA-15 as a function of the weight loss of the same sample. The number p of H/D atoms/nm^2 after increasing the drying period is added at the top of the figure. The initial wet sample (with proton intensity 1 (au)) is not shown. Spectra for p below 30 are shown in Figure 6.

and a repetition delay of 600 s. The chemical shift ppm scale referred to tetramethylsilane. Proton decoupling was employed during the acquisition, using the TPPM scheme with 70 kHz decoupling power and $\Delta\varphi = \pm 17°$. In all experiments, the data points of the free induction decay signals were left shifted to the first rotational echo position prior to the Fourier transform.

Results and Discussion

Drying of the Inner Surface of SBA-15. ***Proton Spectra.*** To characterize the exchange motion of the alanine molecules and its dependence on the number of water molecules present inside the channels, we begin with characterizing the water contents in our samples. In this section, we will restrict ourselves to experiments on SBA-15 samples. To characterize the water distribution in these samples and to compare our proton spectra with those reported in the literature, we loaded a sample with a 50:50 wt % H_2O/D_2O mixture. The water was removed in a stepwise fashion by pumping the NMR sample in a vacuum line, and the weight of the sample was measured at each stage. ^{1}H and ^{2}H spectra were recorded, and the resulting line shapes were integrated and correlated to their weight. A linear dependence between the integrated intensity of both deuterium and proton spectra and the weight change of the sample was obtained, as can be seen in Figure 5. The weight of the samples was measured with an accuracy of 0.1 mg, and the deviation of the proton data points from a straight line in this figure is about 0.25 mg. Assuming that (i) during the drying process, only water is removed and that the H_2O/D_2O ratio stays constant in the sample; (ii) all protons in the sample contribute to the spectral intensities; and (iii) the surface area per gram of SBA-15 is known, we can derive for each proton spectrum a p value for the number of protons per square nanometer of surface as presented in Figure 6a. Extrapolation of the straight lines in Figure 5 to zero intensity enables us to determine the amount of dry SBA-15 in the rotor. This value was 22.5 mg, which corresponds (using the data of Table 1) to a total pore surface area of 1.9×10^{19} nm^2. An uptake of 8 mg of water, corresponding to 0.22×10^{-3} mol of H_2O and 0.2×10^{-3} mol of D_2O, resulted in a change in integrated proton/deuterium intensity of 0.45/0.72 a.u., respectively, and a p value of 26 H/D's per nm^2. The reproducibility of our integrated intensity and weight measurements indicate that the inaccuracy of our p values is about ± 1.5. For that reason, we will present p values only as integers. For all other samples, the reported p values were determined in the same way as discussed here.

In Figure 6a room temperature ^{1}H spectra are shown as a function of p. When the sample is relatively wet ($p = 23$), the ^{1}H spectrum consists of at least two overlapping lines: one corresponding to bulk water at ~4.9 ppm and one around 4 ppm. The latter corresponds to water molecules located around surface oxygen sites at the surface. Drying the sample to a level up to $p = 10$ moves the maximum of this line toward ~3.5 ppm and removes the line with a maximum at ~4.9 ppm. Starting at this p value, additional spectral features between 8 and 2 ppm become significant. From the overall line shape, it follows that we are dealing with some distribution of clusters of different sizes. Below $p = 10$, we can clearly observe additional types of protons: multiproton clusters of different sizes with chemical shift values that are determined by the exchange between bound −OH and H_2O protons, isolated −OH groups at 1.8 ppm, and acidic protons around 7 ppm. The difference in the spectral components can also be demonstrated by measuring T_2 relaxation times as a function of the position in the spectrum. According to these measurements (not shown), the intrinsic line width of the cluster lines is about 2−3 ppm, meaning that we are dealing with a set of components originating from different clusters. The distribution of cluster sizes is not known at this stage, but the inhomogeneity of the overall line shape indicates that the clusters are isolated from each other. All these findings are consistent with the results reported by Grunberg et al. Their spectral line widths are smaller than in our spectra, suggesting that in our SBA-15 samples, the pore surfaces are less crystalline and contain a higher concentration of silica islands.[30]

The relative intensity of the peak corresponding to the silanol −OH protons in the driest sample is about 50%. This corresponds to about 2−3 isolated −OH/OD groups/nm^2, when we take into account that $p = 5$. The remaining average number of H/D per nm^2 is then 3, which can be attributed to at least one (−OH + H_2O/D_2O) cluster/nm^2 with a chemical shift value around 3.4−3.9 ppm. Here, we assume that the silanol protons inside the walls between the pores are only a minor fraction of the total number of protons in the sample. For increasing p values, the line around 7 ppm is clearly present.

The low concentration of isolated oxygen sites that are protonated in the driest sample can be confirmed by ^{29}Si NMR measurements. A spin−echo ^{29}Si spectrum was measured and analyzed in terms of the relative intensities of the Q^3 line at −100 ppm and the Q^4 line at −110 ppm. The ratio between the two integrated intensities of these lines is 3:7. Combining this ratio with the pore volume and diameter obtained from the N_2 adsorption measurements (summarized in table 1), we find that the estimated number of Si−O−H sites per square nanometer of the inner surface is about 3.5. When all water protons are located around surface oxygen sites and p varies from 5 to 23, the cluster sizes vary between 1 and at least 6. No Q^2 line was obtained, as can be seen in the ^{29}Si spectrum in the Supporting Information.

The ^{1}H MAS spectra show some first-order side bands with intensities that are less than 10% of the centerband at a spinning frequency of 10 kHz. This suggests that the homonuclear interaction between neighboring protons is rather small and we are dealing with coupled protons that experience fast exchange between positions in the clusters. At this stage, we did not perform a deconvolution of the spectra for increasing p values.

Deuterium Spectra. To determine the dynamic character of the protons in our sample, we also measured ^{2}H MAS spectra of D_2O residing in the pores. In Figure 6b, these ^{2}H spectra are shown as a function of p. Above $p = 10$, a single line composes

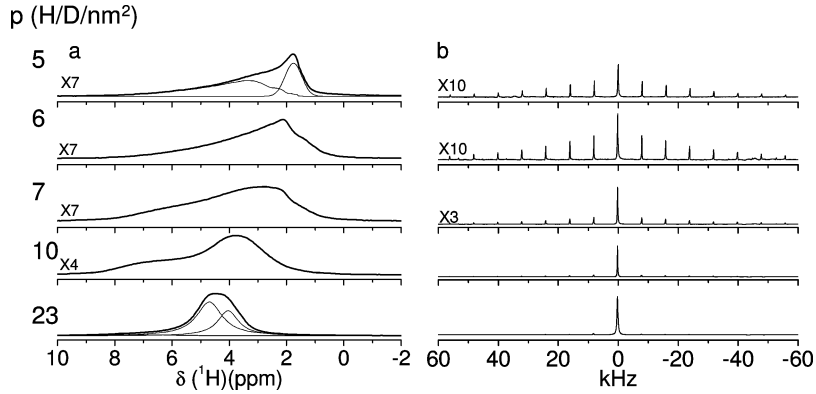

Figure 6. Corresponding room temperature ^{1}H (a) and ^{2}H (b) MAS spectra of a sample containing a 1:1 H_2O/D_2O mixture inside SBA-15 at different stages of drying. The values of p are given on the left.

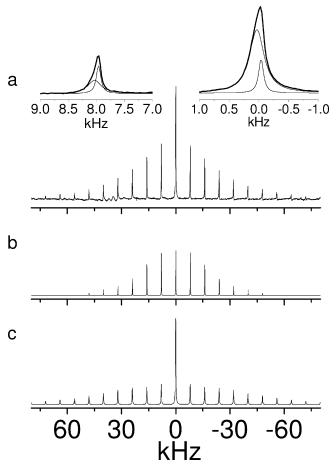

Figure 7. (a) The room temperature ^{2}H MAS spectrum of SBA-15 (without alanine) with $p = 5$. (b,c) The narrow-line (23%) and broad-line (77%) components of this experimental spectrum, after spectral deconvolution. The inserts present a closer look at the centerband and the first sideband, showing the narrow- and broad-line components.

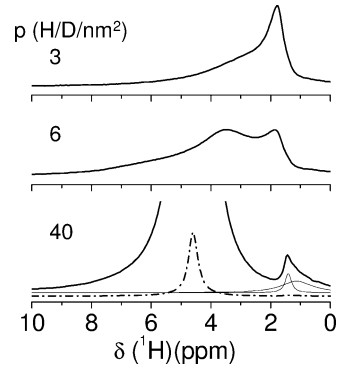

Figure 8. The room temperature ^{1}H MAS spectra of a SBA-15 sample loaded with a 1:1 H_2O/D_2O solution of alanine-h_3 at different p values. The p values are indicated on the left. The spectra are presented with the same spectral amplification. The shape of the main lines for $p = 40$ (dotted line), reduced by a factor of 30 with respect to the solid-line spectrum, is also shown.

the spectrum, indicating that all deuterium atoms perform some reorientational motion. Below this value, a narrow sideband pattern appears in the spectra. A careful analysis shows that each band is composed of two lines. As a result, the spectrum of the driest sample could be decomposed into two sideband patterns, as shown in Figure 7: a pattern with individual line widths of about 100 Hz and a frequency spread of ±50 kHz and a pattern with 400 Hz line width and a frequency spread of ±70 kHz. Comparing these spectra with the two components of the proton spectrum of $p = 5$ in Figure 6a suggests that the narrow ^{2}H spectrum corresponds to Si−OD groups and the broader sideband spectrum to the residual proton clusters, positioned at a lower field in the proton spectra. The relative integrated intensities of the two sideband patterns are 1:3. A best-fit procedure to the MAS spectra with static quadrupole parameters (ν_Q, η) resulted in the values (51 kHz, 0) for the narrow-line spectrum. Single-OD groups, performing a fast rotational motion around their Si−O bond with a Si−O−D angle of 47°, are expected to result in a $\eta = 0$ spectrum with a quadrupole coupling constant of about 51 kHz. The centerband of the broad-line spectrum is relatively high, indicating that this spectrum belongs to water protons experiencing some exchange motion. Ignoring this centerband intensity and assuming static parameters, the broad-line spectrum can be simulated with (ν_Q, η) = (90 kHz, 0.5). These parameters are significantly smaller than ∼ 216 kHz, the value of ice.[63] Correlating the broad-line part of the ^{2}H spectrum to the low field component of the ^{1}H spectrum, we must conclude that their protons/deuterons are positioned in small clusters (presumably with $x = 3$). Exchange between the water and OH protons together with the presence of a set of oriented water−OH configurations at the surface make it impractical to try to fit the broad-line ^{2}H spectrum using an exchange model. At p values well above 10, the spectrum turns into a single spectral band, indicating that the protons are no longer localized in small clusters and that their dynamic behavior approaches the random orientational motion of bulk water.

Addition of Alanine to the Sample. To examine whether the guest molecules remain in the sample during the removal of the solvent, we loaded a sample of SBA-15 with a solution of nondeuterated alanine (alanine-h_3) in a 1:1 H_2O/D_2O mixture with a concentration of 0.18 mM. Assuming that the pores are fully loaded with the solution at the preparation stage, taking the pore surface of 849.22 m^2/g for SBA-15 into account, this concentration corresponds to about 0.2 alanine molecules/nm^2. During a drying procedure, ^{1}H NMR spectra were recorded at different p values, as shown in Figure 8. These spectra are drawn at the same order of magnitude to follow the dependence of the intensities of the methyl lines of alanine on p. At $p = 40$, the methyl protons of alanine are clearly observed and show two lines: a line at 1.4 ppm and a broader line at 1.2 ppm. These results suggest that we are dealing with at least two alanine populations. Apparently, one with alanine in an aqueous environment and one with alanine interacting with the surface. The origin of a shift of ∼0.2 ppm with respect to the common methyl line of alanine at 1.4 ppm is not clear yet. Additional

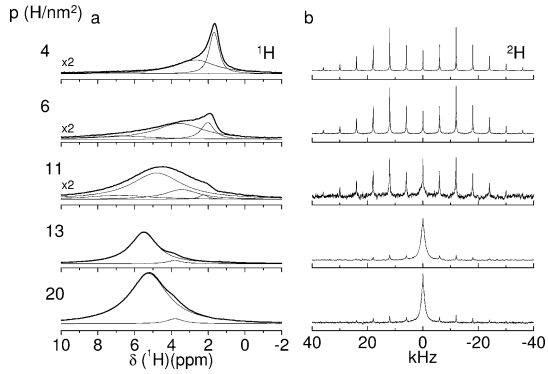

Figure 9. Normalized room temperature ^{1}H (a) and ^{2}H (b) MAS spectra of a sample of alanine-d_3 dissolved in water inside SBA-15 after different drying periods with the p values as indicated on the left.

drying causes both lines to disappear. The fact that they disappear from the spectrum after additional drying must be correlated with the restrictions in the reorientational motion of the alanine molecules. The spectral features observed around 6−7 ppm at $p = 6$ should not necessarily be attributed to alanine. The line intensity at these ppm values was also observed in spectra of SBA-15 samples that did not contain alanine.

The possibility that alanine molecules are removed from the sample during the water evaporation was ruled out by adding water to the driest sample. The resulting ^{1}H spectrum at a fully water-loaded sample again showed two methyl alanine lines with the same chemical shifts and intensities as the lines in the spectrum before the drying procedure. We can thus be sure that, although the guest molecules undergo different binding dynamics, they remain in the sample at all stages of the drying process.

When the −OH line appears at low p values, it seems that most alanine molecules stick to the surface, resulting in the disappearance of their methyl proton line in the spectrum. Here, we must remind ourselves that all proton spectra were collected using an echo sequence, suppressing very broad spectral features, such as baselines distortions and static proton line shapes. In the driest sample, the proton−OH line intensity corresponds to about 2 isolated −OH/−OD groups/nm^2. Comparing the relative intensities of these −OH lines and the CH_3 protons, the upper bound of the number of alanine molecules per square nanometer can be estimated as 0.2. This value agrees well with the amount of alanine inserted into the sample during preparation.

From the proton and deuterium data up to this point, we can conclude that we are able to detect the effects of very small proton clusters. These clusters are spatially structured, and their presence influences the dynamics of the alanine molecules. To achieve a better understanding of this motion, we will now present dynamic ^{2}H MAS spectra of deuterated alanine-d_3 as a function of p and temperature and combine these results with spectra of the protons in the pores. Line fitting of the ^{2}H MAS spectra using the two-site exchange model will provide us with the average values of the desorption rate constants, $k_{bf}(p; T)$, and the fraction of bound guest molecules, $P_b(p; T)$. Correlation between these parameters and the cluster distribution will be discussed.

Dynamic Studies during Drying. ***Proton Spectra.*** A sample of SBA-15 loaded with a solution of alanine-d_3 in H_2O was gradually dried under vacuum, and ^{1}H and ^{2}H MAS spectra were recorded as a function of p. In this set of experiments, the number of alanine molecules per square nanometer was again much smaller than 1. Figure 9a shows ^{1}H spectra at various p values. At $p = 20$, the proton spectrum consists mainly of a single, broad line shape with a maximum at about 5 ppm and a small contribution at ∼3.8 ppm. Comparing this spectrum with the $p = 23$ spectrum in Figure 6a indicates that we are again dealing with two main contributions; however, their relative intensities are different. The presence of the main line at $p = 20$ as well as at $p = 13$ suggests that most of the protons are not localized and that there is a fast exchange between the water molecules belonging to different clusters. When there are about 3 oxygen binding sites/nm^2 at the pore walls, the average cluster size varies from 4 to 7. The spectra indicate that there is a fast exchange of water molecules already when the cluster size becomes larger than 4.

Around $p = 11$, a shift of the main line to higher field is observed, and a line at 7 ppm appears. Lowering the water content in the sample to a lower level results in the appearance of the −OH line at 1.8 ppm. A similar p dependence was already reported by Grunberg et al.[30] Assuming that the intrinsic linewidths of the spectral components are a few ppm, a reasonable data-fitting can be obtained by combining four main components: a line for the −OH groups with a maximum at ∼(1.8−2) ppm, two broad lines around ∼(2.7−3.5) and ∼(4.4−5.4) ppm, and an additional line around ∼(6.8−7) ppm. Such an analysis is performed on the spectra of Figure 9a. The reduction of the lines at ∼(4.4−5.4) ppm, corresponding to bulk water and large clusters, and the appearance of the smaller ones at ∼(2.7−3.5) and ∼(6.8 − 7) ppm are clearly observed during the drying procedure.

Deuterium Spectra. After having characterized the water loading as a function of p, we will now analyze the deuterium MAS spectra shown in Figure 9b. These spectra change significantly during the drying process. All MAS spectra could be deconvoluted in terms of two MAS sideband patterns. One narrow line band pattern with varying overall intensity corresponds to the static spectrum of the CD_3 group of those alanine-d_3 that are fixed to the pore surface and possess a ν_Q value of 51 kHz (not shown). The other broad-line part of the spectra changes its shape during the drying process; it corresponds to those alanine-d_3 molecules that participate in an exchange process. These broad-line sideband spectra are analyzed using the two-site exchange model to retrieve the dynamic parameters (Figure 10b). These spectral patterns were obtained by deconvolution of the experimental spectra and fitting all individual center and sidebands to a Lorenzian line shape. Very small corrections were applied to the resulting spectra in order to symmetrize their overall shape.

From the relative center and sideband intensities of the static narrow line spectra, we determined the relative amount of fixed surface-bound guest molecules $S_b(p)$. The dynamic spectra were compared to calculated ones and resulted in the average parameters $P_b(p)$ and $k_{bf}(p)$, as can be observed in Figure 10c and summarized in Figure 11 and Table 2. The values of $k_{bf}(p)$ vary between 0.5 and 160 × 10^3 s^{-1}. The P_b and S_b dependences on p, as drawn in Figure 11, show some two-state transition between dynamic processes with high p values and low P_b and S_b values and processes with low p values and high P_b and S_b values. The transition between the two types of processes appears around $p = 12$. The p dependence of log (k_{bf}) appears, unexpectedly, to be close to linear.

Realizing that the spectra can also be a superposition of a set of spectra with a distribution of parameters $\{k_{bf}, P_b\}$, we can determine only average rate constants, $k_{bf}(p)$, and relative populations, $P_b(p)$. The deviations between spectra that are simulated, based on one pair of average parameters, and based on a summation of a distribution of spectra with different

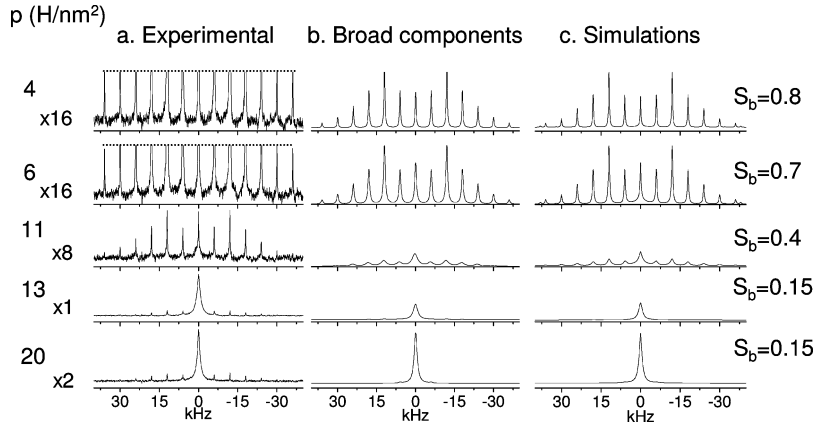

Figure 10. Experimental ^{2}H MAS spectra of alanine-d_3 in a sample of SBA-15 at different p values. (a) The actual spectra are shown. Each spectrum is amplified to show its different components, and the multiplication factors are chosen with respect to the $p = 13$ spectrum. The amplification causes truncation at the top of part of the spectra. (b) The broad-line components, obtained after deconvolution of all individual center and sidebands and symmetrization of the spectra, are shown. The overall shapes of all narrow-line spectra possess the static sideband pattern of a CD_3 group with $\nu_Q = 51$ kHz. (c) The best-fit simulated spectra. As expected, the simulated line shapes are not Lorentzian. The S_b values are added on the figure, and the resulting dynamic parameters are at $p = 20$, ($k_{bf} = 160 \times 10^3$ s^{-1}, $P_b = 0.1$); at $p = 13$, ($k_{bf} = 15 \times 10^3$ s^{-1}, $P_b = 0.3$); at $p = 11$, ($k_{bf} = 5 \times 10^3$ s^{-1}, $P_b = 0.7$); at $p = 6$, ($k_{bf} = 1.2 \times 10^3$ s^{-1}, $P_b = 0.9$); and at $p = 4$, ($k_{bf} = 0.7 \times 10^3$ s^{-1}, $P_b = 0.95$).

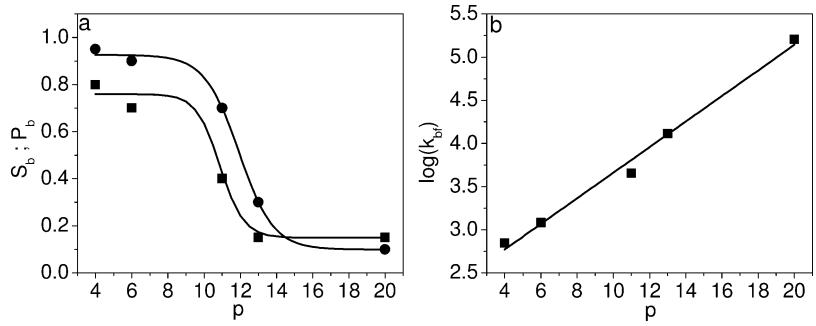

Figure 11. (a) The S_b (squares) and P_b (circles) values of bound alanine-d_3 molecules in a sample of SBA-15, as well as the log(k_{bf}) values as a function of p in (b). The lines are drawn for eye guidance only and to demonstrate the possible similarity between the dependence of S_b and P_b on p.

TABLE 2: Values of S_b, P_b, and k_{bf} Derived from the Analysis of the ^{2}H MAS Spectra Using the Two-Site Exchange Model, for Alanine-d_3 Inside SBA-15 at Different p Values

p	S_b	P_b	k_{bf} (s^{-1})	% −OH
4	0.8	0.95	0.7×10^3	35
6	0.7	0.9	1.2×10^3	15
11	0.4	0.7	5×10^3	2
13	0.15	0.3	15×10^3	0
20	0.15	0.1	160×10^3	0

TABLE 3: The Integrated Intensities $I(p,x)$ (in a.u.) of the Different Spectral Components, Obtained from the Deconvolution of ^{1}H Spectra of the SBA-15 Sample Loaded with Alanine-d_3 at Different p Values[a]

p	1.8−2.0 ppm	2.7−3.5 ppm	4.4−5.4 ppm	6.8−7.0 ppm	total
4−5	180	280		30	490
6	100	360		100	560
11	20	160	700	120	1000
20		80	1920		2000

[a] The total intensities on the right show some correlation to $100 \times p$.

parameters, depend on the spread of the parameters. In our case, we succeeded in obtaining good best fit parameters using one pair of parameters {k_{bf}, P_b}, realizing that the signal-to-noise ratio of our actual spectra does not justify any additional fine-tuning of these parameters. To investigate this, we conducted a set of simulations to show the similarity between spectra calculated with a single pair of parameters and a small distribution of parameters. An example can be found in the Supporting Information.

Quantitative Data Analysis. Combining the results obtained from the analysis of the proton and deuterium data, we can now try to visualize the dynamics of alanine at low water concentrations. As mentioned earlier, the ^{1}H spectra in Figure 9a can be deconvoluted in terms of four lines around ∼(1.8−2), ∼(2.7−3.5), ∼(4.4−5.4), and ∼(6.8−7.0) ppm. All these lines are broad, with fwhh around 2−3 ppm. Therefore, the results of this deconvolution cannot be very accurate. However, they provide an overall picture of the changes in the spectrum during drying. The deconvolution was done manually, and the values of the line intensities, widths, and positions can be determined with an accuracy of only ∼15%. Their integrated intensities in some arbitrary units are summarized in Table 3. These units were chosen in such a way that they can be correlated to the number of protons, $100 \times p$, per 100 nm^2. This was done by assigning the intensity of the lines for $p = 20$ to 2000 a.u. All other intensities are calibrated to this value.

Whereas the line at ∼(1.8−2.0) ppm can be attributed to the −OH protons, the line around 4.4−5.4 ppm corresponds to water clusters with $x \geq 4$ protons and bulk water diffusing on the surface of the pores. A possible assignment of the two additional peaks requires that each one belongs to a single or a small range of cluster sizes. An estimation of these sizes can be obtained when we assume that for $p < 12$, all protons are located close

TABLE 4: The Number of Oxygen Sites $N(p, x)$ Occupied by x Protons for Each Value of p on a Surface Area of ~100 nm^2[a]

	$N(4, x)$	$N(6, x)$	$N(11, x)$	$N(20, x)$
(1.8 − 2.0) ppm $x = 1$	180	100	20	
(6.8 − 7.0) ppm $x = 2$	15	50	60	
(2.7 − 3.5) ppm $x = 3$	95	120	55	30
(4.4 − 5.4) ppm $x \geq 4$			175	480[b]
$N_O(p)$	290	270	310	
$(d(1) + d(2) + d(3))/N_O(p)$	1	1	0.40	

[a] The numbers correspond to the intensities $I(p, x)$ in Table 3 according to: $N(p, x) = I(p, x)/x$. The assignment of the spectral component to the values of x are shown in the first column. $N_O(p) = \sum_x N(p, x)$ corresponds to the total number of clusters/100 nm^2. The fractions of sites with less than four protons are shown in the last row. [b] * For $p = 20$ most cluster sizes are larger than 4.

to one of the oxygen sites at the surface and that the number of oxygen sites is about constant. Under these conditions, we can suggest a cluster size distribution $d(p, x)$; that is, the relative number of oxygen sites occupied by x protons for each p value. This is summarized in Table 4 and repeated in the histogram shown in the Supporting Information. Here, we assigned the lines at ~(2.7−3.5) ppm to a single water molecule exchanging with a −OH proton ($x = 3$) and the line at ~(6.8−7) ppm to $-(OH_2)^+$ groups. This last assignment is derived from the appearance and assignment of these groups in SBA-15 samples that are synthesized in an acidic environment by the use of HCl, as in our case.[12] The different surface sites and their ^{1}H chemical shift assignments are schematically presented in Figure 1. This assignment is, of course, a global picture of the real system, in which at least some single water migration is always present. The line positions of the $x = n$ clusters, which contain one −OH group and $(n - 1)/2$ exchanging H_2O molecules, depend on the chemical shift of the protons in the possible cluster configurations and the proton exchange rates between the proton sites of these configurations. If the chemical shifts are determined only by their typical values 1.8 and 5 ppm, the line positions of the clusters in the fast exchange limit are ~3.9 and ~4.3 ppm for $n = 3$ and 5, respectively. For example, for $n = 3$, different conformations can result in average chemical shift values that can be as low as 2.9 ppm.[30] In the framework of our assignment, the total number of oxygen sites occupied by x protons $N(p, x)$ is expected to be equal to $d(p, x)/N_O$, where N_O is the total number of oxygen sites. Its value is estimated to be ~300/100 nm^2. The spectrum at $p = 20$ consists mainly of one line that must be attributed to cluster sizes larger than 4 or bulk surface water.

To get a better understanding of the dynamic behavior of the alanine molecules, we must correlate the relative values of fixed molecules $S_b(p)$ with those of $d(p; x)/N_0$. For the low concentrations of alanine (about 50 molecules/100 nm^2 in our case), we can assume that each of these molecules is located on the inner pore surface close to one of the oxygen sites. It is important to mention that the bound alanine molecules do not exhibit any reorientational motion except the methyl rotation. This follows from the fact that the effective quadrupole coupling constant of the bound alanine molecules is 51 kHz, which is an average value that results from the methyl groups' rotating around their fixed CD_3 symmetry axes. This indicates that the binding of the alanine molecules to the surface is not only via their NH_2 or NH_3^+ group and that an additional (hydrogen) bond is needed to restrict the molecule from rotating around its C_α−N bond.

At $p = 4$ and 6, almost all alanine molecules are fixed to the surface, meaning that the number of free water molecules is not sufficient to cause alanine removal, even part of the time. The small proton clusters ($x \leq 3$) are not contributing enough water molecules to exchange with the alanine molecules. This changes when the clusters become larger, but are still partially isolated, as for $p = 11$. Then, there seems to be enough water molecules available to initiate the exchange process. The coexistence of the (4.4−5.4) ppm and the other lines in the proton spectrum led us to conclude that we are also dealing with surface areas with clusters of size $x > 3$ and other areas with $x \leq 3$. The fact that the deuterium spectrum at $p = 11$ does not show a narrow line at the center suggests that the alanine molecules in the first areas are not reorienting freely in an aqueous environment; moreover, the larger clusters contribute enough water molecules to start a dynamic process on only 60% ($S_b(11) = 0.4$) of the surface. The changes in the values of $\{k_{bf}(p), P_b(p)\}$ as a function of p also suggest that the kinetics is changing according to the number of available water molecules and according to their rate of appearance at a fixed alanine site. At $p = 20$, all protons belong in clusters with sizes that are larger than or equal to 4. Then, there are hardly any stationary alanines left in the sample ($S_b = 0.1$). These dynamic alanine molecules are experiencing an increasing rate constant, but they do not yet seem to diffuse isotopically. Whether this exchange motion is combined with some restricted translational

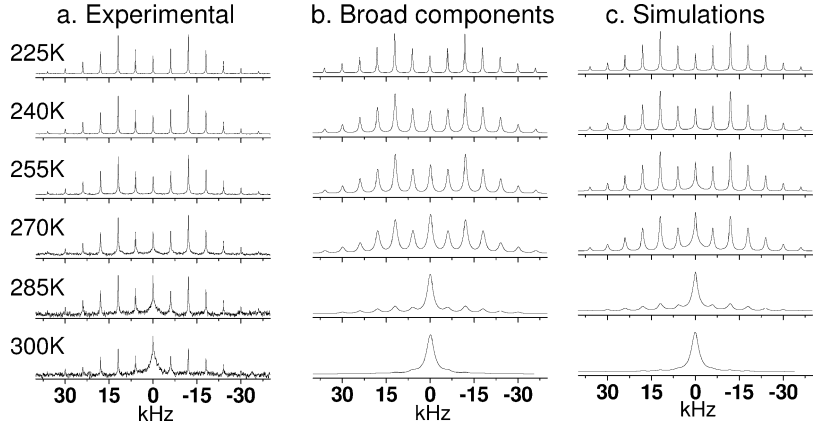

Figure 12. (a) ^{2}H MAS experimental spectra of alanine-d_3 in a sample of SBA-15 with $p = 12$ at different temperatures. The normalized broad-line component of these spectra, obtained by deconvolution (b), are compared with their best-fit simulated spectra (c). The resulting dynamic parameters are at 300 K, ($k_{bf} = 27 \times 10^3$ s^{-1}, $P_b = 0.3$); at 285 K, ($k_{bf} = 7 \times 10^3$ s^{-1}, $P_b = 0.6$); at 270 K, ($k_{bf} = 3 \times 10^3$ s^{-1}, $P_b = 0.8$); at 255 K, ($k_{bf} = 1.3 \times 10^3$ s^{-1}, $P_b = 0.87$); at 240 K, ($k_{bf} = 1 \times 10^3$ s^{-1}, $P_b = 0.92$); and at 225 K, ($k_{bf} = 0.6 \times 10^3$ s^{-1}, $P_b = 0.99$).

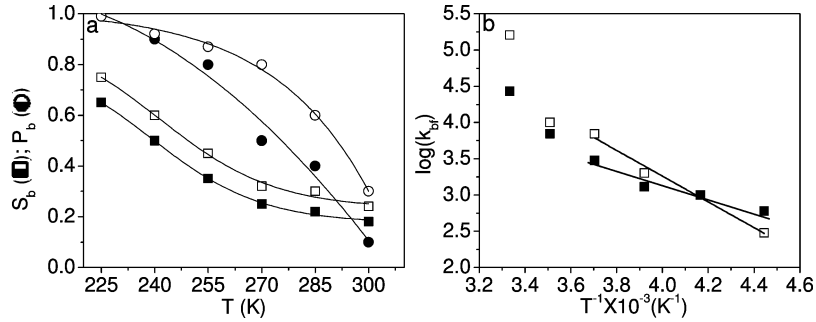

Figure 13. (a) The S_b (squares) and P_b (circles) values of bound alanine-d_3 molecules in a sample of SBA-15 as a function of T as well as the log(k_{bf}) values as a function of $1/T$ (b) are drawn for samples with $p = 12$ (open shapes) and $p = 20$ (closed shapes). The lines are only for eye guidance and to demonstrate the possible similarity of the T dependences of S_b and P_b. The straight lines in part b, through the low temperature values of log(k_{bf}), correspond to activation energies of 4 and 8 kcal/mol for $p = 12$ and 20, respectively, assuming an Arrhenius temperature dependence.

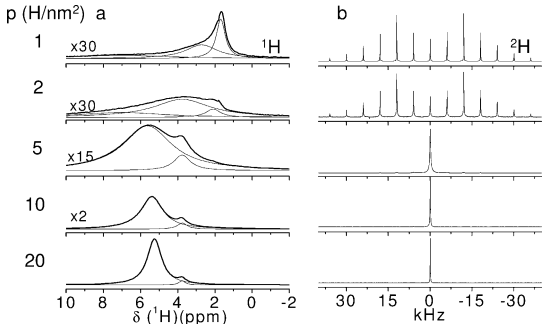

Figure 14. Room temperature normalized ^{1}H (a) and ^{2}H (b) MAS spectra of a sample of MCM-41 loaded with a H_2O solution of alanine-d_3 after different drying periods, with p values as indicated. To show the relative intensities of the actual proton spectra, the amplification factors with respect to the spectrum with $p = 20$ are added.

TABLE 5: The Integrated Intensities of the Different Spectral Components Derived from Deconvolution of ^{1}H Spectra of MCM-41 Loaded with Alanine-d_3 at Different p Values[a]

	1.8−2.0	2.7−3.5	4.4−5.4	6.8−7.0	total
$p = 1,2$	40, 20	40, 100		30, 40	110, 160
$p = 5$		60	450		510
$p = 10$		80	960		1040
$p = 20$		80	1920		2000

[a] The intensities are presented in arbitrary units that are convenient for the discussion. The overall intensities on the right can be correlated to the values of $100 \times p$.

motion over the surface cannot be determined by our experiments. This description of the dynamic process of alanine is consistent with the deuterium data from the H_2O/D_2O loaded sample. There, we found that above $p = 7$, part of the deuterons lose their localization and start diffusing over the surface.

In conclusion, we can say that the exchange motion of the alanines depends on the availability of single water molecules. At low p values (<4), the small clusters do not provide these water molecules, but for increasing values of p (≥4), the clusters are not confined enough and contribute *single* free water molecules. Whether the change in the alanine exchange parameters is caused by an increase in the number of free water molecules on the surface only or also by an increase in the diffusion rate of the single water molecules over the surface is not clear.

Temperature Dependence in SBA-15 and MCM-41. ***Alanine-d_3 Inside SBA-15.*** *Proton Spectra.* In this section, we discuss the temperature dependence of the proton and deuterium

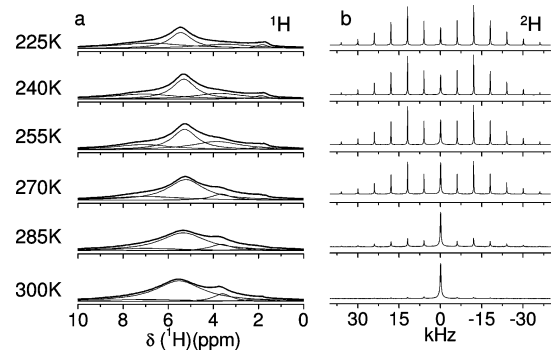

Figure 15. Normalized ^{1}H (a) and ^{2}H (b) MAS spectra of a sample of MCM-41 loaded with a H_2O solution of alanine-d_3 with $p = 3$ at different temperatures.

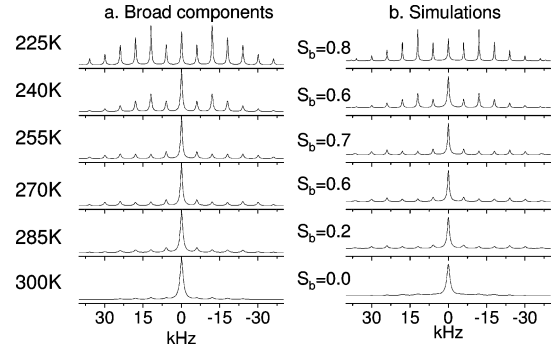

Figure 16. The normalized broad-line components of ^{2}H MAS spectra of alanine-d_3 inside MCM-41 with $p = 3$ at different temperatures (obtained by deconvolution) (a) are compared with their corresponding best-fit simulated spectra (b). The relative values of bound alanines, S_b, in the samples are derived from the experimental spectra and added, as well. The resulting dynamic parameters are at 300 K, ($k_{bf} = 9 \times 10^3$ s^{-1}, $P_b = 0.35$); at 285 K, ($k_{bf} = 4 \times 10^3$ s^{-1}, $P_b = 0.55$); at 270 K, ($k_{bf} = 2.3 \times 10^3$ s^{-1}, $P_b = 0.6$); at 255 K, ($k_{bf} = 1.7 \times 10^3$ s^{-1}, $P_b = 0.65$); at 240 K, ($k_{bf} = 1.5 \times 10^3$ s^{-1}, $P_b = 0.7$); and at 225 K, ($k_{bf} = 0.5 \times 10^3$ s^{-1}, $P_b = 0.99$).

spectra. We start with two SBA-15 samples loaded with alanine-d_3. The p values of these samples were 12 and 20. The first sample was chosen to represent the intermediate case, in which at ambient temperatures, there are enough water molecules to cause part of the alanine molecules to exchange with free water molecules. In the second sample, there are enough water molecules to remove all the alanine molecules from the surface most of the time. The proton spectra as a function of temperature are shown together with their compositions in the Supporting Information. These spectra lose their total integrated intensity with temperature reduction mainly due to the change in the line

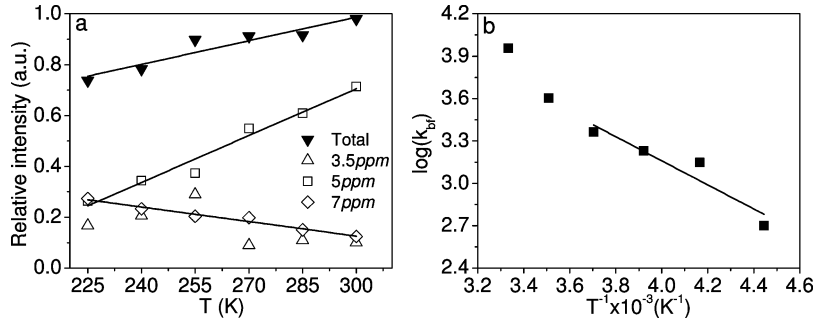

Figure 17. (a) The relative integrated intensities of the different ^{1}H MAS spectral components at different temperatures, derived from deconvolution of the proton spectra, as well as the log(k_{bf}) values as a function of $1/T$ (b), of a sample of alanine-d_3, dissolved in H_2O, inside MCM-41 with $p = 3$. The lines are for eye guidance only. The straight line in part b, through the low-temperature values of log (k_{bf}), corresponds to an activation energy of 4 kcal/mol, assuming an Arrhenius temperature dependence.

intensity at (4.4−5.4) ppm. Nevertheless, the lines at (6.8−7) ppm and (2.7−3.5) ppm become more pronounced. Thus, the larger clusters and bulk water solidify, and the relative number of smaller clusters is maintained or even increases. As a result, we expect the number of water molecules available for alanine exchange to decrease.

Due to the assumption that the alanine molecules are randomly located between the proton clusters, we expect the relative number of bound alanines $S_b(p; T)$ to increase and the k_{bf} rates to decrease (without taking into account thermal activation) when the temperature is reduced. These general features can be inspected by following the temperature dependence of the deuterium MAS spectra of the alanine-d_3 molecules.

Deuterium Spectra. The temperature-dependent deuterium spectra of alanine-d_3 inside SBA-15 with $p = 12$ are shown in Figure 12. The spectra of the $p = 20$ samples are shown in the Supporting Information. These spectra were deconvoluted in terms of a narrow-line sideband pattern corresponding to static guest molecules and a dynamic spectrum. The fitting parameters for these dynamic spectra are given in the figure captions.

As predicted, the $S_b(p; T)$ values increase with decreasing temperature, as can be seen in Figure 13. The temperature dependences of the $P_b(p; T)$ values as well as of $k_{bf}(p; T)$ are also shown in this figure. The $P_b(p; T)$ values increase for decreasing temperature, whereas at each temperature, they are smaller for the $p = 20$ sample than for the $p = 12$ sample. There are more free water molecules available in the sample with $p = 20$ than in the one with $p = 12$, even at temperatures below 270 K. The temperature dependence of log(k_{bf}) is not linear as a function of the reciprocal temperature.

An Arrhenius temperature dependence of $k_{bf}(p; T)$ is not expected for the overall temperature range. Nevertheless, if the thermal activation of the alanine−water exchange can be defined by some binding energy difference to the surface, we can expect that the dependence of k_{bf} can be written as

$$k_{bf}(p;T) = A(P_b(p;T))e^{-E_{bf}/kT} \quad (14)$$

where the prefactor is a function of the dynamics and concentration of the free water molecules. In our two-site model, this dependence reflects itself in changes in the value of the parameter $P_b(p; T)$. At the low temperature range, below 270 K, the P_b value does not change significantly and approaches 1. Under these conditions, the temperature dependences of log($k_{bf}(p; T)$ seem to be close to linear with effective activation energies of about 4 and 8 ± 1 kcal/mol for $p = 12$ and 20, respectively.

We must, however, conclude that the difference in binding energies between alanine and water at the oxygen sites cannot be determined from the $k_{bf}(T)$ dependence. In future studies, we may approach the interpretation of the complex exchange dynamics of the alanine−water system close to a −OH site by initiating molecular dynamics calculations.

Alanine-d_3 inside MCM-41. A temperature study similar to SBA-15 was performed on alanine-d_3 in an aqueous environment inside MCM-41. The pore diameter in MCM-41 is significantly smaller than that of SBA-15, and its inner pore surface is better defined crystallographically. We therefore expect that the density of silanol sites and small clusters, $x < 4$, is much lower in MCM-41 than in SBA-15. This manifested itself immediately during the drying process. By correlating the weight loss to the total intensity of the proton spectra, we were again able to determine p values for the number of protons per square nanometer using the surface area per gram given in Table 1. The changes in the proton and deuterium spectra of alanine-d_3 as a function of p are shown in Figure 14.

The deviations in the ratios between the weight loss of the sample and the proton line intensity restricts the accuracy of the p values to more than 1. For example, the weight reduction during sample drying, going from stage $p = 2$ to stage $p = 1$, is only 6%. Thus, for these samples, we will consider the total intensities of the proton signals, and not p, as a measure of the difference between the two samples. Table 5 summarizes these intensities, again choosing arbitrary units that resemble the average number of protons per 100 nm^2. The difference between the spectra of the two driest samples is, however, significant. It emphasizes the variability of the spectra in terms of possible redistributions between the small clusters at low concentrations. In Figure 14a, we see that at $p = 20$, almost all (95%) protons are located around 5 ppm and that the deuterium spectrum shows an isotropic line. This changes gradually with a disappearance of the proton line at 5 ppm. Below $p = 5$, the two contributions around 2 and 7 ppm appear in the spectra. In terms of our earlier assignment of the spectral bands, assuming it is also valid here, the large clusters and bulk water disappear below $p = 5$, and at $p = 2$, 1, all residual water molecules are located in small clusters with $x \leq 3$. For $p = 1$, 2, the number of −OH sites at the driest sample is about 25 on an area of 100 nm^2; the number of $x = 2$ clusters, (6.8−7.0) ppm, assumed to belong to a small number of acid protons, is about 15; and the $x = 3$ clusters, about 20. Together with this trend, the free water molecules, able to exchange with the alanine molecules, disappear below $p = 5$, and we do not expect any alanine−water exchange anymore.

The deuterium spectra are again analyzed as before. Above $p = 5$, we do not observe any static deuterium spectrum of alanine-d_3. The spectrum at $p = 5$ has still a value of zero for S_b, and all alanine molecules are dynamic, with an average desorption rate of 8×10^3 s^{-1} and an average P_b value of 0.3. This situation changes when we reduce the water contents by only 2 water molecules/nm^2. Then we observe the chemical shifts of the small clusters (~3 and 7 ppm), and the deuterium spectrum approaches its static shape. The deuterium spectrum at the lowest p value can be deconvoluted in a static sideband pattern and a dynamic spectrum with parameters $\{S_b = 0.8; P_b = 0.99; k_{bf} = 0.5 \times 10^3$ s$^{-1}\}$ for the $p = 1$ spectrum. The transition from mobile ($S_b \approx 0$) to bound alanine molecules ($S_b \approx 1$) is consistent with the changes in the proton spectra.

We can thus conclude that in MCM-41, the density of oxygen binding sites is very low and that only at very low water concentrations do the alanine molecules become static due to lack of free water molecules.

The low concentration of surface sites reduces the possibility of alanine molecules' being mobile at low temperatures. In Figure 15, the proton and deuterium spectra of the MCM-41 sample, loaded with alanine-d_3 with $p = 3$ protons/nm^2, are shown as a function of temperature. The two-site exchange model was again used to analyze the dynamic spectra, and the fitting of the spectra is shown in Figure 16, together with the k_{bf} and P_b values in the figure caption. When analyzing the proton spectra, the first observation is that the total intensity of the proton spectra decreases by only 20% when the sample is cooled to 225 K; this is shown in Figure 17a. The larger clusters and bulk water freeze, and the small clusters stay dynamic, without allowing any free water molecules. Around 270 K, most of the alanine molecules, which were dynamic at room temperature, become immobile. This can clearly be observed by the sharp increase of S_b at that temperature. When we assume that it is allowed to use an Arrhenius $1/T$ dependence of $\log(k_{bf})$ at the low temperature range, an average activation energy value of 4 ± 1 kcal/mol is obtained as can be seen in Figure 17b. At our lowest temperature (225 K), the deuterium spectrum is similar to that of the driest sample at ambient temperature, when there are hardly any clusters available in which an exchange process can take place. Thus, here, we also cannot determine experimentally the energy difference between alanine and water binding.

Conclusions

The mobility of alanine molecules on the inner surface of the mesoporous materials is strongly dependent on the characteristics of the surfaces. Moreover, the concentration and dynamics of water molecules near the surface also has a strong effect on the behavior of the guests. For high oxygen-cluster densities, a significant part of the alanine molecules can perform only local exchange motion when there are enough unbound single water molecules floating at the surface. We would expect that according to the hydrophobic character of an ideal, dry silica surface, it prefers the water molecules to be clustered at the surface binding sites. However, already at clusters larger than $x = 4$, molecules start to migrate over the surface. In the case of SBA-15, this stage is reached when p becomes about 11, and for MCM-41, at much lower p values, around 3. Realizing that the number of oxygen binding sites per square nanometer is about 3 and around 1, respectively, the number of water molecules per square nanometer needed to start the water−alanine exchange process must be about 3 and 1. As a result, the changes in the dynamic behavior in MCM-41 occurs much earlier. For example, a change from $p = 2$ to $p = 3$ causes a significant change in the dynamic character of the alanine molecules (from static to dynamic), as observed in the deuterium spectra. Thus, single water molecules are sufficient to exchange with the alanine molecules. The concentration of oxygen binding sites determines the number of single water molecules necessary for the exchange process to occur. The difference between the surface wetting properties of the SBA-15 and MCM-41 samples can be one of the surface characteristics that supports the different drying mechanisms of these systems, as reported by Grunberg et al.[30]

Acknowledgment. We thank Prof. Miron Landau for providing us with the mesoporous materials and Dr. Raphy Poupko for providing us with the program for line shape simulation in the presence of MAS and dynamics. We also thank Dr. A.J. Vega and Prof. Asher Schmidt and his group for fruitful discussions. This study has been supported by a grant of the Minerva Foundation. This research is made possible in part by the historic generosity of the Harold Perlman family.

Supporting Information Available: Additional information as noted in text. This material is available free of charge via the Internet at http://pubs.acs.org.

References and Notes

(1) Jing, H.; Xiaofen, L.; Evans, D. J.; Xue, D.; Chengyue, L. *J. Mol. Catal.* **2000**, *11*, 45.
(2) Haruo, T.; Bo, L.; Toshiya, S.; Chie, M.; Tsutomu, K.; Shinji, I. *Microporous Mesoporous Mater.* **2001**, *44*, 755.
(3) Pages, G.; Delaurent, C.; Caldarelli, S. *Anal. Chem.* **2006**, *78* (2), 561–566.
(4) Yurong, M. L. Q.; Jiming, M.; Yongqing, W. O. L.; Huming, C. *Colloids Surf., A* **2003**, *229*, 1.
(5) Ladizhansky, V.; Hodes, G.; Vega, S. *J. Phys. Chem. B* **1998**, *102*, 8505.
(6) Ladizhansky, V.; Hodes, G.; Vega, S. *J. Phys. Chem. B* **2000**, *104*, 1939.
(7) Vallet-Regi, M.; Ruiz-Gonzalez, L.; Izquierdo-Barba, I.; Gonzalez-Calbet, J. M. *J. Mater. Chem.* **2006**, *16*, 26–31.
(8) Horcajada, P.; Ramila, A.; Ferey, G.; Vallet-Regi, M. *Solid State Sci.* **2006**, *8*, 1243–1249.
(9) Beck, J. S.; Vartuli, J. C.; Roth, W. J.; Leonowicz, M. E.; Kresge, C. T.; Schmitt, K. D.; Chu, C. T.; Olson, D. H.; Sheppard, E. W.; McCullen, S. B.; Higgins, J. B.; Schlenker, L. J. *J. Am. Chem. Soc.* **1992**, *114*, 10834–10843.
(10) Huo, Q.; Margolese, D. I.; Ciesla, U.; Feng, P.; Gier, T. E.; Sieger, P.; Leon, R.; Petroff, P. M.; Schuth, F.; Stucky, G. D. *Nature (London)* **1994**, *368*, 317.
(11) Shenderovich, I. G.; Buntkowsky, G.; Schreiber, A.; Gedat, E.; Sharif, S.; Albrecht, H.; Golubev, N. S.; Findenegg, G. H.; Limbach, H. H. *J. Phys. Chem. B* **2003**, *107*, 11924–11939.
(12) Baccile, N.; Laurent, G.; Bonhomme, C.; Innocenzi, P.; Babonneau, F. *Chem. Mater.* **2007**, *19*, 6–1343.
(13) Nawrocki, J. *J. Chromatogr., A* **1997**, *779*, 29–71.
(14) Zhuravlev, L. T. *Colloids Surf., A* **2000**, *173*, 1.
(15) Shi, L.; Zou, Y.; He, H. *Chem. Lett.* **2001**, 1164.
(16) Chuang, I.; Maciel, G. E. *J. Am. Chem. Soc.* **1996**, *118*, 401–406.
(17) Courivaud, F.; Hansen, E. W.; Kolboe, S.; Karlsson, A.; Stocker, M. *Microporous Mesoporous Mater.* **2000**, *37*, 223.
(18) Zhang, W.; Ratcliffe, C. I.; Moudrakovski, I. L.; Tse, J. S.; Mou, C.; Ripmeester, J. H. *Microporous Mesoporous Mater.* **2005**, *79*, 195.
(19) Qiao, S. Z.; Bhatia, S. K. *Ind. Eng. Chem. Res.* **2005**, *44*, 6477.
(20) Okazaki, M.; Toriyama, K.; Anandan, S. *Chem. Phys. Lett.* **2005**, *401*, 363.
(21) Gedat, E.; Schreiber, A.; Albrecht, J.; Emmler, T.; Shenderovich, I.; Findenegg, G. H.; Limbach, H. H.; Buntkowsky, G. *J. Phys. Chem. B* **2002**, *106*, 1977.
(22) Stallmach, F.; Graser, A.; Karger, J.; Krause, C.; Jeschke, M.; Oberhagemann, U.; Spange, S. *Microporous Mesoporous Mater.* **2001**, *4* (4−45), 745.
(23) Nguyen, C.; Sonwane, C. G.; Bhatia, S. K.; Do, D. D. *Langmuir* **1998**, *14*, 4950.
(24) Masierak, W.; Emmler, T.; Gedat, E.; Schreiber, A.; Findenegg, G. H.; Buntkowsky, G. *J. Phys. Chem. B* **2004**, *108*, 18890.

(25) Aksnes, D. W.; Forland, K.; Stocker, M. *Microporous Mesoporous Mater.* **2005**, *77*, 79.
(26) Vyalikh, A.; Emmler, Th.; Shenderovich, Y. Z.; Findenegg, G. H.; Buntkowsky, G. *Phys. Chem. Chem. Phys.* **2007**, *9*, 2249–2257.
(27) Henchman, R. H.; McCammon, J. A. *Protein Sci.* **2002**, *11*, 2080–2090.
(28) Pujadas, G.; Palau, J. *Protein Sci.* **2001**, *10*, 1645–1657.
(29) Cauvel, A.; Brunel, D.; Di Renzo, F. *Langmuir* **1997**, *13*, 2773–2778.
(30) Grunberg, B.; Emmler, T.; Gedat, E.; Shenderovich, I.; Findenegg, G. H.; Limbach, H.; Buntkowsky, G. *Chem.—Eur. J.* **2004**, *10*, 5689.
(31) Takahara, S.; Nakano, M.; Kittaka, S.; Kuroda, Y.; Mori, T.; Hamano, H.; Yamaguchi, T. *J. Phys. Chem. B* **1999**, *103*, 5814.
(32) Morishige, K.; Kawano, K. *J. Chem. Phys.* **1999**, *110* (10), 4867.
(33) Schreiber, A.; Ketelsen, I.; Findenegg, G. H. *Phys. Chem. Chem. Phys.* **2001**, *3*, 1185.
(34) Helms, V. *Chem. Phys. Chem.* **2007**, *8*, 23–33.
(35) Duer, M. J. *Introduction to Solid State NMR Spectroscopy*; Blackwell Publishing Ltd: Malden, MA, 2004.
(36) Schmidt-Rohr, K.; Spiess, H. W. *Multidimensional Solid-State NMR and Polymers*; Academic Press: London, San Diego, 1994.
(37) Wiench, J. W.; Bronnimann, C. E.; Lin, S. Y.; Pruski, M. *J. Am. Chem. Soc.* **2007**, *129* (40), 12076.
(38) Trebosk, J.; Wiench, J. W.; Huh, S.; Lin, S. Y.; Pruski, M. *J. Am. Chem. Soc.* **2005**, *127* (9), 3057.
(39) Luz, Z.; Poupko, R.; Alexander, S. *J. Chem. Phys.* **1993**, *99*, 7544.
(40) Pizzanelli, S.; Kababya, S.; Frydman, V.; Landau, M.; Vega, S. *J. Phys. Chem. B* **2005**, *109*, 8029.
(41) Geil, B.; Isort, O.; Boddenbery, B.; Favre, D. E.; Chmelka, B. F.; Fujara, F. *J. Chem. Phys.* **2002**, *116*, 2184.
(42) Kristensen, J. H.; Hoatson, G. L.; Vold, R. L. *J. Chem. Phys.* **1999**, *110* (9), 4533.
(43) Okazaki, M.; Toriyama, K. *J. Phys. Chem. B* **2003**, *107*, 7654.
(44) Azais, T.; Tourne-Peteilh, C.; Aussenac, F.; Baccile, N.; Coelho, C.; Devoisselle, J. M.; Babonneau, F. *Chem. Mater.* **2006**, *18*, 6382–6390.
(45) Perea, W.; Cannella, M.; Yang, J.; Vega, A. J.; Polenova, T.; Marcolongo, M. *Magn. Reson. Med.* **2007**, *57*, 990.
(46) Goetz, J. M.; Hoatson, G. L.; Vold, R. L. *J. Chem. Phys.* **1992**, *97*, 1306.
(47) Halle, B. *Prog. Nucl. Magn. Reson. Spectrosc.* **1996**, *28*, 137–159.
(48) Halle, B. *Magn. Reson. Med.* **2006**, *56*, 60–72.
(49) Spiess, H. W. *Colloid Polym. Sci.* **1983**, *261*, 193–209.
(50) Poupko, R.; Luz, Z. *J. Chem. Phys.* **1981**, *75* (4), 1675.
(51) Smith, R. L.; Oldfield, E. *Science* **1984**, *225* (4659), 280–288.
(52) Kustanovich, I.; Vega, S.; Zaborowski, E. *J. Magn. Reson.* **1991**, *93* (2), 441–446.
(53) Huang, Y.; Vold, R. L.; Hoatson, G. L. *J. Chem. Phys.* **2006**, *124*, 104504.
(54) Vega, S. *Nuclear Magnetic Resonance Probes of Molecular Dynamics*; Kluwer Academic Publishers: Dordrecht, Boston, 1994.
(55) Mittermaier, A.; Kay, L. E. *J. Am. Chem. Soc.* **1999**, *121* (45), 10608–10613.
(56) Schmidt, A.; Smith, S. O.; Raleigh, D. P.; Roberts, J. E.; Griffin, R. G.; Vega, S. *J. Chem. Phys.* **1986**, *85* (8), 4248.
(57) Schmidt, A.; Vega, S. *J. Chem. Phys.* **1987**, *87*, 6895.
(58) Boender, G. J.; Vega, S.; De Groot, H. J. M. *Mol. Phys.* **1998**, *95*, 921.
(59) Massiot, D.; Fayon, F.; Capron, M.; King, I.; Le Calve, S.; Alonso, B.; Durand, J.-O.; Bujoli, B.; Gan, Z.; Hoaston, G. *Magn. Reson. Chem.* **2002**, *40*, 70–76.
(60) Vradman, L.; Landau, M. V.; Herskowitz, M.; Ezersky, V.; Talianker, M.; Nikitenko, S.; Koltypin, Y.; Gedanken, A. *J. Catal.* **2003**, *213*, 163–175.
(61) Landau, M. V.; Varkey, S. P.; Herskowitz, M.; Regev, O.; Pevzner, S.; Sen, T.; Luz, Z. *Microporous Mesoporous Mater.* **1999**, *33*, 149–163.
(62) Bielecki, A.; Burum, D. P. *J. Magn. Reson., A* **1995**, *116*, 215–220.
(63) Wittebort, R. J.; Usha, M. G.; Ruben, D. J.; Wemmer, D. E.; Pines, A. *J. Am. Chem. Soc.* **1988**, *110* (17), 5668–5671.

JP810572R